Dalton Transactions

ROYAL SOCIETY OF CHEMISTRY

PAPER

View Article Online
View Journal | View Issue

Open Access Article. Published on 25 July 2022. Downloaded on 1/21/2026 6:06:26 AM.
This article is licensed under a Creative Commons Attribution-NonCommercial 3.0 Unported Licence.

Check for updates

Cite this: *Dalton Trans.*, 2022, **51**, 12334

Cyclometalated iridium complexes based on monodentate aminophosphanes†

Marco Palmese, Jesús J. Pérez-Torrente and Vincenzo Passarelli *

Received 29th June 2022,
Accepted 22nd July 2022

DOI: 10.1039/d2dt02081e

rsc.li/dalton

Monodentate aminophosphanes HNP [NH(4-tolyl)PPh_2] and $SiMe_3$NP [$SiMe_3$N(4-tolyl)PPh_2] react with [Ir(μ-Cl)(cod)]$_2$ affording tetra- or pentacoordinate complexes of formula [IrCl(L)$_n$(cod)] (L = HNP, n = 1, 2; L = $SiMe_3$NP, n = 1). The reaction of [IrCl($SiMe_3$NP)(cod)] with carbon monoxide smoothly renders [Ir(CO)$_3$($SiMe_3$NP)$_2$][IrCl$_2$(CO)$_2$]. The reaction of HNP or $SiMe_3$NP with [Ir(CH_3CN)$_2$(cod)][PF_6] yields the cyclometalated iridium(III)-hydride derivatives [IrH{κ^2*C*,*P*-NR(4-$C_6H_3CH_3$)PPh_2}(cod)(CH_3CN)][PF_6] (R = H, $SiMe_3$) as a result of the intramolecular oxidative addition of the tolyl C^2–H bond to iridium. The straighforward formation of [IrH{κ^2*C*,*P*-$SiMe_3$N(4-$C_6H_3CH_3$)PPh_2}(cod)(CH_3CN)]$^+$ was observed when the reaction was monitored by NMR spectroscopy at 233 K, whereas a more complex reaction sequence was observed in the formation of [IrH{κ^2*C*,*P*-NH(4-$C_6H_3CH_3$)PPh_2}(cod)(CH_3CN)]$^+$, including the formation of [IrH{κ^2*C*,*P*-NH(4-$C_6H_3CH_3$)PPh_2}(HNP)(cod)]$^+$ and [Ir(cod)(HNP)$_2$]$^+$. The "mixed" complex [IrH{κ^2*C*,*P*-$SiMe_3$N(4-$C_6H_3CH_3$)PPh_2}(HNP)(cod)]$^+$ was obtained upon reaction of [IrH{κ^2*C*,*P*-NH(4-$C_6H_3CH_3$)PPh_2}(cod)(CH_3CN)][PF_6] with $SiMe_3$NP at 233 K. Finally, the reaction of [Ir(CH_3CN)$_2$(coe)$_2$][PF_6] with $SiMe_3$NP or HNP resulted in the formation of [Ir(CH_3CN)$_2$($SiMe_3$NP)$_2$][PF_6] and [IrH{κ^2*C*,*P*-NH(4-$C_6H_3CH_3$)PPh_2}(HNP)$_2$(CH_3CN)][PF_6], respectively. Both the *OC*-6-35 and the *OC*-6-52 isomers of [IrH{κ^2*C*,*P*-NH(4-$C_6H_3CH_3$)PPh_2}(HNP)$_2$(CH_3CN)]$^+$ – featuring facial and meridional dispositions of the phosphorus atoms, respectively – were isolated depending on the reaction solvent. Several compounds described herein catalyse the dehydrogenation of formic acid in DMF, [IrCl(HNP)$_2$(cod)] being the most active, with TOF$_{1\ min}$ of about 2300 h^{-1} (5 mol% catalyst, 50 mol% sodium formate, DMF, 80 °C).

Introduction

Ligand design is a longstanding, generally accepted strategy which allows for the preparation of new compounds with tailored properties. In this regard, aminophosphanes have been attracting attention due to their modular synthesis from amines and chlorophosphanes,[1] allowing facile structural modifications. As far as aminophosphanes of general formula $NHRPR_2$ or NR_2PR_2 are concerned, different coordination modes have been reported, so far (Scheme 1). As a matter of fact, in mononuclear complexes, the expected monodentate κ*P* coordination[2] has been observed along with the η^2 coordination,[3] whereas the 1κ*N*,2κ*P* coordination[4] has been reported in dinuclear complexes (Scheme 1-top). Additionally, a very limited number of examples of κ^2*C*,*P* cyclometalated aminophosphano ligands have been reported, when NR_2 is *N*-indolyl[5a,b] or *N*-carbazolyl,[5b] or in the case that a phenyl group[2f,5c] is attached to nitrogen (Scheme 1-bottom). In these cases, a five member metalacycle M–P–N–C–C forms as a result of the CH activation. Interestingly, aminophosphano

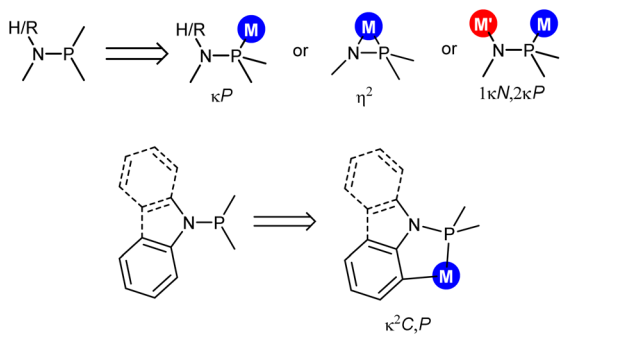

Scheme 1 Coordination modes of aminophosphanes $NHRPR_2$ or NR_2PR_2.

Departamento de Química Inorgánica, Instituto de Síntesis Química y Catálisis Homogénea (ISQCH), Universidad de Zaragoza-CSIC, C/Pedro Cerbuna 12, ES-50009 Zaragoza, Spain. E-mail: passarel@unizar.es

†Electronic supplementary information (ESI) available: Crystal structures, IR and NMR spectra, NMR data, coordinates of calculated structures. CCDC 2178753–2178757. For ESI and crystallographic data in CIF or other electronic format see DOI: https://doi.org/10.1039/d2dt02081e

This journal is © The Royal Society of Chemistry 2022

Open Access Article. Published on 25 July 2022. Downloaded on 1/21/2026 6:06:26 AM.
This article is licensed under a Creative Commons Attribution-NonCommercial 3.0 Unported Licence.

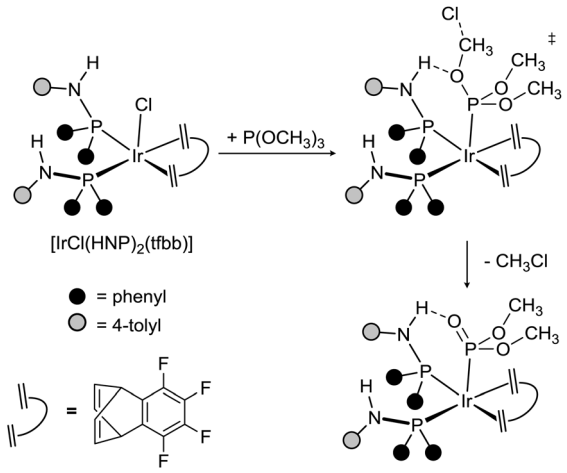

Scheme 2 Reaction of $[IrCl(HNP)_2(tfbb)]$ with trimethyl phosphite.[2a]

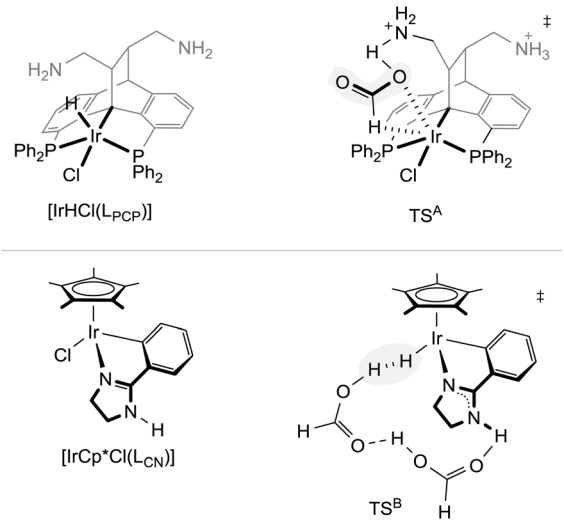

Fig. 1 Selected iridium catalysts (left) for the formic acid dehydrogenation and related transition states (right).[6d,g,i]

complexes have found application as drugs,[2d] catalysts,[2b,g,3a,b] and redox-active multimetallic systems.[4e,h]

Relevant to this paper, we have recently described[2a] the synthesis of the iridium(I) complex $[IrCl(HNP)_2(tfbb)]$ [HNP = NH(4-tolyl)PPh_2; tfbb = tetrafluorobenzobarrelene] and its reaction with trimethyl phosphite, reporting that one of the peripheral NH groups is able to establish an intramolecular NH···O hydrogen bond that triggers the elimination of methylchloride and the formation of the phosphonato complex $[Ir\{PO(OMe)_2\}(HNP)_2(tfbb)]$, thus showing that the HNP-Ir scaffold is able to activate small molecules *via* hydrogen bonding (Scheme 2).[2a]

With this in mind, we envisioned that Ir-HNP derivatives could act as catalysts for the dehydrogenation of formic acid. Actually, a number of homogeneous catalysts based on iridium[6] have proved to be extremely active, and mechanistic studies have revealed that hydrogen bonds between peripheral NH groups and formic acid play a crucial role in stabilizing both intermediates and transition states involved in the formation of dihydrogen and/or carbon monoxide.[7] As an example, Fig. 1 shows the transition states TS^A and TS^B proposed for the dehydrogenation of formic acid catalysed by $[IrHCl(L_{PCP})]$[6d] and $[IrCp^*Cl(L_{CN})]$,[6g,i] respectively, highlighting the role of NH ancillary groups in the formation of both carbon dioxide (TS^A) or dihydrogen (TS^B).

On this background, we decided to delve into the preparation of new iridium complexes with the aminophosphano ligand NH(4-tolyl)PPh_2 (HNP) and its silylated analogue $SiMe_3$N(4-tolyl)PPh_2 ($SiMe_3$NP). Specifically, herein we describe the synthesis of iridium(I) complexes of formula $[IrCl(RNP)_n(cod)]$ (R = H, $SiMe_3$; n = 1, 2) as well as cyclometalated iridium(III) derivatives resulting from the intramolecular CH oxidative addition of the C^2–H bond of the tolyl group to the iridium centre. In addition, a selection of the prepared complexes has been tested as catalysts for the dehydrogenation of formic acid, guessing that the peripheral NH group(s) might foster the catalytic process.

Results and discussion

Synthesis of $SiMe_3$N(4-tolyl)PPh_2 ($SiMe_3$NP)

The synthesis of $SiMe_3$N(4-tolyl)PPh_2 ($SiMe_3$NP) was carried out following a route similar to that reported for $SiMe_2\{N(4\text{-tolyl})PPh_2\}_2$.[8] Indeed, the parent aminophosphane NH(4-tolyl)PPh_2 was sequentially treated with *n*-BuLi and $SiMe_3Cl$ affording $SiMe_3$NP (Scheme 3). As a consequence of the H/$SiMe_3$ substitution, a well-shaped ^1H doublet is observed at 0.47 ppm for the $SiMe_3$ moiety ($^4J_{HP}$ = 1.0 Hz) instead of the ^1H signal of the NH hydrogen atom of HNP, and a significant downfield shift of the $^{31}P\{^1H\}$ NMR signal of $SiMe_3$NP (δ_P 50.5 ppm) with respect to HNP (δ_P 28.7 ppm) was observed.

The crystal structure of $SiMe_3$NP (Fig. 2) shows an almost planar geometry of the nitrogen atom $[\Sigma^\circ_N = 355(2)^\circ]$ and an almost perpendicular arrangement of the C16–C17–C18–C19–C20–C21 aromatic ring with respect to the nitrogen plane [Si–N–C16–C17 −116.94(10)°]. Also, bond lengths Si–N [1.7574(10) Å], P–N [1.7167(10) Å] and C16–N [1.4383(14) Å] are similar to those reported for the related aminophosphane $SiMe_2\{N(4\text{-tolyl})PPh_2\}_2$ (Si–N 1.751 Å, av.; P–N 1.723 Å, av.; C–N 1.446 Å, av.).[9] On these grounds, similar to what proposed for $SiMe_2\{N(4\text{-tolyl})PPh_2\}_2$, back-donation should exist mainly between nitrogen and phosphorus and should primarily be

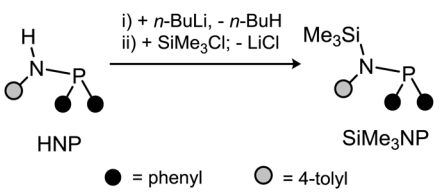

Scheme 3 Synthesis of $SiMe_3$NP.

Open Access Article. Published on 25 July 2022. Downloaded on 1/21/2026 6:06:26 AM.
This article is licensed under a Creative Commons Attribution-NonCommercial 3.0 Unported Licence.

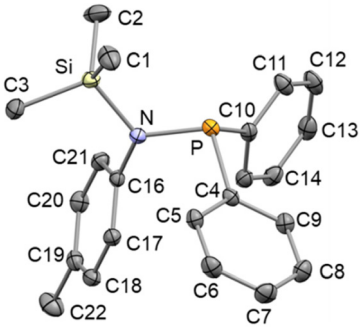

Fig. 2 ORTEP plot of $SiMe_3N(4\text{-tolyl})PPh_2$ ($SiMe_3NP$). Hydrogen atoms are omitted for clarity and thermal ellipsoids are at 50% probability. Selected bond lengths (Å) and angles (°) are: P–N 1.7167(10), Si–N 1.7574(10), N–C16 1.4383(14), C16–N–P 122.30(7), C16–N–Si 118.88(7), P–N–Si 117.22(5), Si–N–C16–C17 –116.94(10).

responsible for the planar geometry of the nitrogen atom in $SiMe_3NP$ (*vide infra*).

Preparation of iridium(I) compounds

Both HNP and $SiMe_3NP$ react with $[Ir(\mu\text{-Cl})(cod)]_2$ (P : Ir = 1) affording the tetracoordinate iridium complexes [IrCl(L)(cod)] (L = HNP, **1**; $SiMe_3NP$, **2**) (Scheme 4).

The crystal structure of **1** and **2** are given in Fig. 3 showing a distorted square planar geometry at iridium with a *cis* disposition of the chlorido and aminophosphano ligands. The coordination environments in **1** and **2** are virtually superimposable, nevertheless **1** and **2** differ in terms of intramolecular short contacts. Indeed, a NH···Cl hydrogen bond was observed in **1**, whereas an anagostic CH···Ir interaction[10] was observed in **2** (Fig. 3). As a consequence, a significantly different dihedral angle Cl–Ir–N–P is observed [**1**, 36.05(13)°; **2**, −51.40(6)°].

The NMR spectra of **1** and **2** suggest that the square planar structure observed in the solid state is preserved in solution. Indeed, for both compounds one $^{31}P\{^1H\}$ NMR signal is

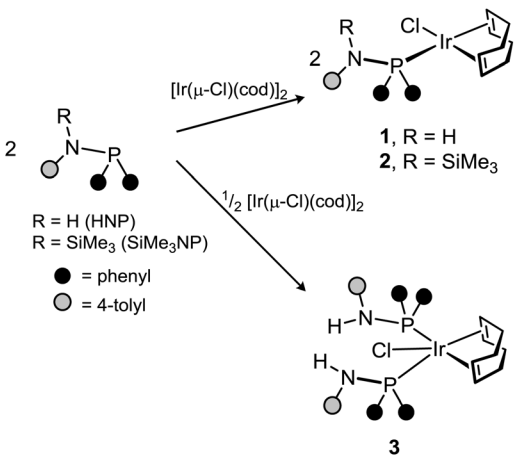

Scheme 4 Reaction of HNP or $SiMe_3NP$ with $[Ir(\mu\text{-Cl})(cod)]_2$.

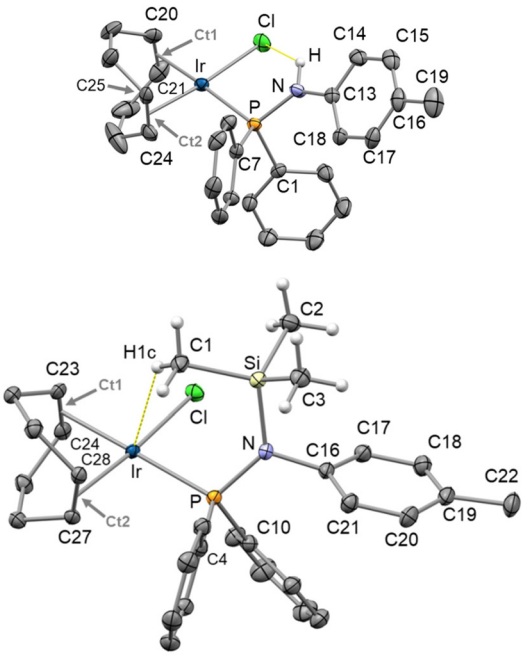

Fig. 3 ORTEP plot of IrCl(cod)(HNP) (**1**, top) and IrCl(cod)($SiMe_3NP$) (**2**, bottom). Most hydrogen atoms are omitted for clarity and thermal ellipsoids are at 50% probability. Selected bond lengths (Å) and angles (°) are: **1**, Ir–P 2.2850(9), Ir–Cl 2.3488(9), P–N 1.675(3), C20–C21 1.384(5), C25–C24 1.414(5), Ir–Ct2 1.98682(17), Ir–Ct1 2.08157(17), N–H 0.96(3), N–C13 1.417(4), P–Ir–Cl 88.31(3), C13–N–P 132.4(3), C13–N–H 113(3), P–N–H 115(3), Cl–Ir–P–N 36.05(13), N–H···Cl hydrogen bond: H···Cl 2.48(4), N···Cl 3.156(3), N–H 0.960(19), Cl–H–N 127(4); Ct1, centroid of C20 and C21; Ct2, centroid of C24 and C25. **2**, N–P 1.6926(12), N–Si 1.7814(12), N–C16 1.4419(18), P–Ir 2.3028(4), Ir–Cl 2.3634(4), C28–C27 1.4260(19), C24–C23 1.394(2), Ct1–Ir 2.08575(16), Ct2–Ir 1.98914(14), P–N–Si 129.23(7), C16–N–P 118.78(9), C16–N–Si 111.98(9), P–Ir–Cl 89.136(12), Ct2–Ir–Ct1 86.812(6), C17–C16–N–Si 83.66(17), N–P–Ir–Cl −51.46(6). CH···Ir contact: H1c···Ir 2.56(3), C1···Ir 3.371(2), C1–H1c 1.076 (19), Ir–H1c–C30 131.1(9). Ct1, centroid of C23 and C24; Ct2, centroid of C27 and C28.

observed (δ_P 43.9, **1**; 62.2 ppm, **2**) along with two olefinic resonances for the cod ligand (δ_H 2.81 and 5.63, **1**; 2.39 and 5.48 ppm, **2**; see ESI, Fig. SI5† for selected NMR data with the proposed assignment).

The pentacoordinate derivative $[IrCl(HNP)_2(cod)]$ (**3**) was obtained when $[Ir(\mu\text{-Cl})(cod)]_2$ was reacted with HNP (Ir : HNP molar ratio 1 : 2, Scheme 4). In contrast, the higher steric hindrance of $SiMe_3NP$ prevents the formation of the pentacoordinate complex $[IrCl(SiMe_3NP)_2(cod)]$, even if $SiMe_3NP$ is added in excess. The ^1H and $^{13}C\{^1H\}$ NMR spectra of **3** indicate that the compound is fluxional in solution even at 213 K. Indeed, at that temperature one broad ^1H resonance was observed for the four olefinic hydrogen atoms of the cod ligand (δ_H 3.37 ppm) and two ^1H resonances at 2.36 and 1.91 ppm for the *endo* and *exo* methylene hydrogen atoms of the cod ligand. By the same token, two $^{13}C\{^1H\}$ resonances at 69.0 ppm (t, $^2J_{CP}$ = 7.5 Hz) and at 32.5 ppm (br) were observed for the olefinic and methylene carbon atoms of the cod ligand. In this regard, DFT calculations indicate that **3** may adopt two stable configur-

This journal is © The Royal Society of Chemistry 2022

Open Access Article. Published on 25 July 2022. Downloaded on 1/21/2026 6:06:26 AM.
This article is licensed under a Creative Commons Attribution-NonCommercial 3.0 Unported Licence.

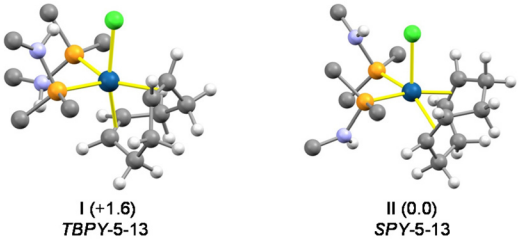

Fig. 4 View of the calculated structures of the *TBPY*-5-13 and *SPY*-5-13 configurations of **3**. The relative Gibbs free energies are given in parentheses (kcal mol^{-1}). For clarity, only *ipso* carbon atoms of tolyl and phenyl groups are shown. Blue, iridium; gray, carbon; orange, phosphorus; green, chlorine; violet, nitrogen; white, hydrogen.

ations, namely *TBPY*-5-13 [11] (**I**,‡ Fig. 4) and *SPY*-5-13 [11] (**II**, Fig. 4), with similar energies (*TBPY*-5-13 → *SPY*-5-13; ΔG = −1.6 kcal mol^{-1}). Thus, reasonably the fast equilibrium *TBPY*-5-13 ⇄ *SPY*-5-13 should exchange the olefinic =CH moieties as well as the CH_2 groups, consequently accounting for the averaged spectra observed for **3**.

The CH···Ir interaction observed in **2** (*vide supra*) is reminiscent of the CH···Ir short contact in the related square planar intermediate [IrCl(SiNP)(CO)][12] resulting from the carbonylation of IrCl(SiNP)(cod) (Scheme 5-top). Taking into account that [IrCl(SiNP)(CO)] smoothly undergoes an intramolecular oxidative addition of the $SiCH_2$–H bond to iridium, the reaction of **2** with CO was carried out, and, in contrast to our expectations, the formation of **4**[$IrCl_2(CO)_2$] was observed (Scheme 5-bottom). The IR spectrum of a CH_2Cl_2 solution of **4**[$IrCl_2(CO)_2$] shows five CO stretching bands (see ESI, Fig. SI3†) confirming the presence of the anion $[IrCl_2(CO)_2]^-$ [2055 (s), 1971 (s) cm^{-1}] and the pentacoordinated cation $\mathbf{4}^+$ [2080 (w), 2008 (s); 1998 (s) cm^{-1}].§ Accordingly, the $^{13}C\{^1H\}$ triplet at 173.5 ppm ($^2J_{CP}$ = 11.1 Hz) and the singlet at 169.1 ppm were assigned to the carbonyl ligands of $\mathbf{4}^+$ and $[IrCl_2(CO)_2]^-$, respectively, and the $^{31}P\{^1H\}$ NMR spectrum contains one singlet at 42.9 ppm. Despite the fact that **4**[$IrCl_2(CO)_2$] is thermally stable in the solid state and was obtained as an analytically pure sample, it is thermally unstable in CD_2Cl_2 and slowly evolves to unidentified species, rendering mixtures still containing about 85 mol% ($^{31}P\{^1H\}$ NMR) of **4**[$IrCl_2(CO)_2$] after 15 h at room temperature.

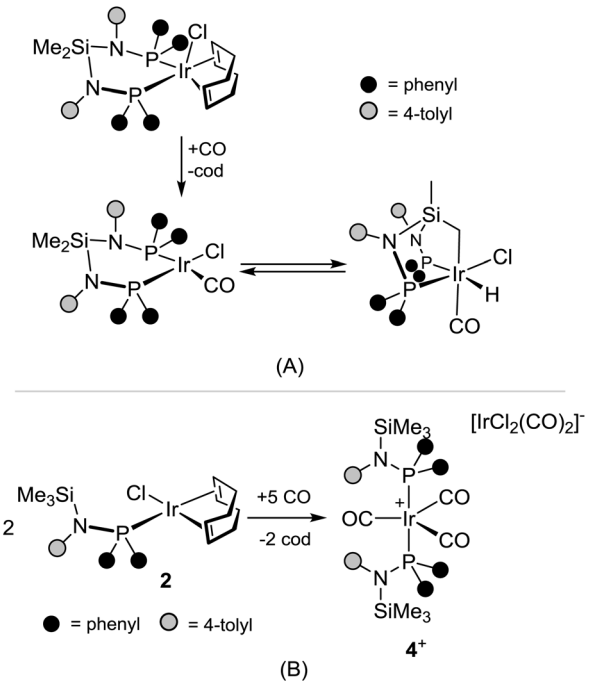

Scheme 5 Carbonylation reaction of [IrCl(SiNP)(cod)] (A, previous work[12]) and [IrCl(SiMe$_3$NP)(cod)] (**2**, B, this work).

Cyclometalation reactions

The reactivity of HNP and $SiMe_3NP$ towards cationic iridium(I) complexes bearing labile ligands has been explored. In the following subsections, the reactions of HNP and $SiMe_3NP$ with $[Ir(CH_3CN)_2(cod)][PF_6]$ or $[Ir(CH_3CN)_2(coe)_2][PF_6]$ will be discussed.

Reactivity with $[Ir(CH_3CN)_2(cod)][PF_6]$. The reaction of HNP or $SiMe_3NP$ with $[Ir(CH_3CN)_2(cod)][PF_6]$ yields the iridium(III) derivatives of formula *OC*-6-24-[IrH{κ^2*C*,*P*-NR(4-$C_6H_3CH_3$)PPh_2}(cod)(CH_3CN)][PF_6] (R = H, **5**PF_6, R = $SiMe_3$, **6**PF_6) resulting from the intramolecular oxidative addition of the tolyl C^2–H bond to iridium (Scheme 6).

The crystal structure of **6**PF_6 was determined by single crystal X-ray diffraction measurements. Its asymmetric unit contains four crystallographically independent pairs of the ions *OC*-6-24-[IrH{κ^2*C*,*P*-$SiMe_3$N(4-$C_6H_3CH_3$)PPh_2}(cod)(CH_3CN)]$^+$ and PF_6^- (see ESI, Fig. SI1†). As for the cations, despite the fact that they are chemically equivalent, they differ in the configuration of the metal centre. Actually, the metal centre of $\mathbf{6}^+$ is stereogenic and two of the cations of the asymmetric unit exhibit *C* configuration[11] at the metal, whereas the remaining two exhibit *A* configuration[11] (ESI, Fig. SI1†). When comparing the cations of the asymmetric unit, related bond

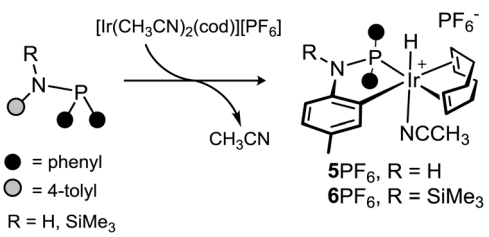

Scheme 6 Formation of **5**PF_6 and **6**PF_6.

‡Note that all non-observed compounds (either expected or calculated) are labelled with sequential roman numerals, whereas sequential arabic numerals have been used exclusively for observed/isolated compounds, including isomers.

§For the sake of comparison, the IR spectrum of the related complex $[Ir(CO)_3(PPh_3)_2]^+$ shows one weak band at 2074 cm^{-1} (A_1 mode) and two strong bands at 2010 and 2018 cm^{-1} (split E mode), *cf.* ref. 34

Open Access Article. Published on 25 July 2022. Downloaded on 1/21/2026 6:06:26 AM.
This article is licensed under a Creative Commons Attribution-NonCommercial 3.0 Unported Licence.

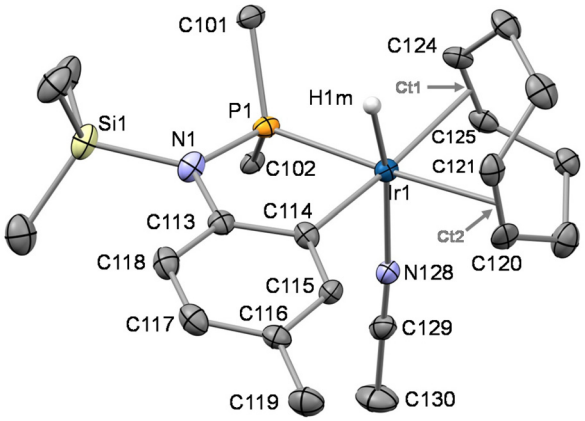

Fig. 5 ORTEP plot of C_{Ir}-*OC*-6-24-[IrH{κ^2*C*,*P*-SiMe$_3$N(4-C$_6$H$_3$CH$_3$)PPh$_2$}(cod)(CH$_3$CN)]$^+$ in **6**PF$_6$. For clarity, most hydrogen atoms are omitted and only the *ipso* carbon atoms of the phenyl groups are shown. Thermal ellipsoids are at 50% probability. Selected bond lengths (Å) and angles (°) are: C114–Ir1 2.075(4), C113–C114 1.410(6), C113–N1 1.455(6), N1–P1 1.681(4), N1–Si1 1.796(4), N128–Ir1 2.127(4), P1–Ir1 2.2640(14), Ir1–H1m 1.596(10), C120–C121 1.390(7), C124–C125 1.380 (6), Ir1–Ct1 2.1909(5), Ir1–Ct2 2.1971(6), C114–Ir1–H1m 80(2), P1–Ir1–H1m 87(2), C114–Ir1–P1 81.14(14), N128–Ir1–H1m 168(2), Ct1–Ir1–Ct2 82.52(2), C113–N1–P1 113.2(3), C113–N1–Si1 121.2(3), P1–N1–Si1 125.5 (2).

lengths and angles are similar, regardless of the configuration at the metal centre. Therefore, for the sake of brevity, only the structure of one of the cation exhibiting *C* configuration (Fig. 5) will be discussed. A distorted octahedral geometry at the metal centre is observed with a *trans* disposition of the hydrido and acetonitrile ligands. The five member Ir1–P1–N1–C113–C114 metallacycle is planar and exhibits a bite angle P1–Ir1–C114 of 81.14(14)° nicely fitting two *cis* coordination sites at the metal centre.

In view of the bond lengths C113–N1 [1.455(6) Å], N1–P1 [1.681(4) Å], and N1–Si1 [1.796(4) Å] and taking into account the planarity of the nitrogen atom N1 [$\Sigma^{\circ}_{N1} = 359.9(8)^{\circ}$], the metalation of the tolyl substituent in **6**$^+$ and the consequent coplanarity of the tolyl moiety and the N1–P1–Si–C113 fragment appear not to bring about any substantial difference in the electronic distribution at the nitrogen atom with respect to SiMe$_3$NP and **2**. In this regard, the delocalization indexes[13] (DI, *aka* Fuzzy Bond Orders, FBO) were calculated for SiMe$_3$NP, **2** and **6**$^+$ (Fig. 6) showing that the nitrogen–phosphorus back-donation is still operative in **6**$^+$ and the nitrogen–carbon bond basically holds its single bond character, similar to SiMe$_3$NP and **2**, where the aromatic ring lies almost perpendicular to the N–Si–C–P plane.

The solution structure of **6**$^+$ is similar to that observed in the solid state. In particular, the ^{1}H signal of the hydrido ligand is a doublet at −16.43 ppm with a $^2J_{HP}$ of 11.2 Hz indicating a mutual *cis* disposition of the hydrido ligand and phosphorus. Also, four non-equivalent olefinic hydrogen atoms are observed for the cod ligand (δ_H 5.54, 5.37, 4.69, 4.09 ppm) and a ^{31}P{^{1}H} singlet is observed at 73.9 ppm downfield-shifted

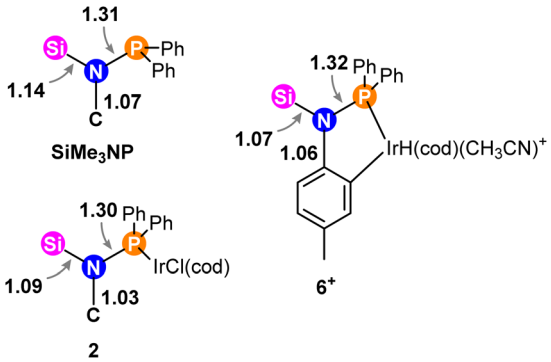

Fig. 6 Delocalization index (DI) for the Si–N, C–N and P–N bonds in SiMe$_3$NP, **2** and **6**$^+$.

with respect to SiMe$_3$NP (50.5 ppm) and **2** (62.2 ppm), reasonably as a consequence of the oxidation state +3 of the metal centre. The metalation of the tolyl group brings about a ^{1}H pattern consisting of two mutually coupled doublets at 7.14 and 6.91 ppm ($^3J_{HH}$ = 8.2 Hz) and one broad singlet at 6.72 ppm assigned to the aromatic hydrogen atoms of the [Ir{κ^2*C*,*P*-SiMe$_3$N(4-C$_6$H$_3$CH$_3$)P}] moiety. Also, the ^{13}C{^{1}H} signal of the metalated carbon atom (δ_C 126.8 ppm) is a doublet as a consequence of the carbon–phosphorus coupling ($^2J_{CP}$ = 3.5 Hz). Finally the ^{1}H singlet at 1.80 ppm indicates the presence of coordinated acetonitrile. The NMR data for **5**PF$_6$ are analogous to those discussed for **6**PF$_6$ suggesting that the solution structure of **5**PF$_6$ should be similar. It is worth a mention that, at variance with **2**, the NH ^{1}H signal of **5**$^+$ is a broad singlet ($\Delta\nu_{1/2}$ = 5.1 Hz) at 5.22 ppm, which suggests that the cyclometalation causes a reduced hydrogen-phosphorus coupling constant. Fig. SI6 (ESI†) shows the detailed assignment of ^{1}H, ^{13}C{^{1}H} and ^{31}P{^{1}H} signals relevant for the solution structure elucidation of **5**$^+$ and **6**$^+$.

The formation of **5**$^+$ and **6**$^+$ was monitored by NMR spectroscopy. In the case of **6**$^+$, the straightforward and clean formation of **6**$^+$ was observed even at 233 K, no intermediate being detected by ^{1}H and ^{31}P{^{1}H} NMR spectroscopy. On the other hand, when monitoring the formation of **5**$^+$, a more complex reaction sequence was brought to light (Scheme 7). Actually, upon adding HNP to [Ir(CH$_3$CN)$_2$(cod)][PF$_6$] (1 : 1 molar ratio) at 233 K,¶ part of [Ir(CH$_3$CN)$_2$(cod)]$^+$ remains unreacted (as seen in the ^{1}H NMR spectrum), whereas HNP reacts completely. In addition, beside **5**$^+$, the square planar complex [Ir(cod)(HNP)$_2$]$^+$ (**7**$^+$) and the hydrido derivative [IrH{κ^2*C*,*P*-NH(4-C$_6$H$_3$CH$_3$)PPh$_2$}(HNP)(cod)]$^+$ (**8**$^+$) were observed (Scheme 7). Fig. 7 shows the ^{31}P{^{1}H} NMR spectrum of the reaction mixture at 233 K along with selected NMR data relevant for the identification of **7**$^+$ and **8**$^+$. Upon raising the temperature up to 298 K (in 10 min approximately), **5**$^+$ is observed in solution as the only product. On these grounds, the reaction

¶A CD$_2$Cl$_2$ (0.5 mL) solution of [Ir(CH$_3$CN)$_2$(cod)][PF$_6$] (0.031 mmol) at 233 K was added with a CD$_2$Cl$_2$ solution (0.5 mL) of HNP (0.031 mmol) and introduced into an NMR spectrometer at 233 K.

This journal is © The Royal Society of Chemistry 2022

Open Access Article. Published on 25 July 2022. Downloaded on 1/21/2026 6:06:26 AM.
This article is licensed under a Creative Commons Attribution-NonCommercial 3.0 Unported Licence.

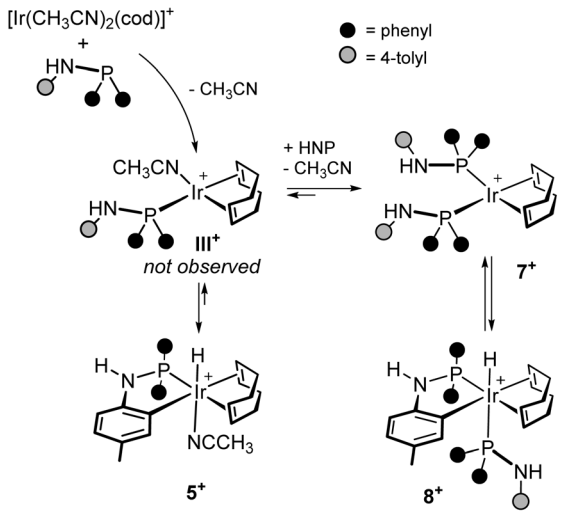

Scheme 7 Reaction sequence for the reaction of $[Ir(CH_3CN)_2(cod)]^+$ with HNP.

of $[Ir(CH_3CN)_2(cod)]^+$ with HNP is likely to yield $\mathbf{5}^+$ reasonably *via* the putative intermediate $[Ir(cod)(HNP)(CH_3CN)]^+$ ($\mathbf{III}^+$) which undergoes an intramolecular CH oxidative addition to iridium (*vide infra*). On the other hand, the formation of $[Ir(cod)(HNP)_2]^+$ ($\mathbf{7}^+$) and $[IrH\{\kappa^2C,P\text{-}HN(4\text{-}C_6H_3CH_3)PPh_2\}(HNP)(cod)]^+$ ($\mathbf{8}^+$) indicates that the putative intermediate $[Ir(cod)(HNP)(CH_3CN)]^+$ ($\mathbf{III}^+$) undergoes a substitution reaction, in which HNP replaces CH_3CN rendering $[Ir(cod)(HNP)_2]^+$ ($\mathbf{7}^+$), which in turn undergoes the intramolecular CH oxidative addition to iridium, yielding $\mathbf{8}^+$.

Admittedly, once formed, $\mathbf{5}^+$ might react with HNP rendering $\mathbf{8}^+$ and releasing CH_3CN (Scheme 7). Nonetheless, the ^1H–^1H EXSY spectrum of the reaction mixture at 233 K shows exchange peaks between $[Ir(cod)(HNP)_2]^+$ ($\mathbf{7}^+$) and $[IrH\{\kappa^2C,P\text{-}HN(4\text{-}C_6H_3CH_3)PPh_2\}(HNP)(cod)]^+$ ($\mathbf{8}^+$) but no exchange peaks have been observed between $\mathbf{8}^+$ and $\mathbf{5}^+$, suggesting that the reaction $\mathbf{5}^+ + HNP \rightarrow \mathbf{8}^+ + CH_3CN$ may not be viable at 233 K whereas the equilibrium $\mathbf{7}^+ \rightleftarrows \mathbf{8}^+$ should be operative at that temperature.‖

Finally, it is worth a mention that the CH oxidative addition to iridium in $\mathbf{1}^+$ is totally regiospecific. In fact, the isomers $\mathbf{IV}^+$ (*OC*-6-25) and $\mathbf{V}^+$ (*OC*-6-35, Fig. 8) were not detected in the reaction mixture. As a confirmation, $\mathbf{IV}^+$ was calculated to be less stable than $\mathbf{5}^+$ (ΔG_{rel} = +6.6 kcal mol^{-1}) whereas the structure of $\mathbf{V}^+$ could not even be located on the potential energy surface (PES), reasonably due to the steric congestion between the PPh_2 moiety and the cod ligand, leading to the dissociation of

‖As far as the equilibrium $\mathbf{7}^+ \rightleftarrows \mathbf{8}^+$ is concerned, ^1H–^1H EXSY crosspeaks have been observed between the following groups of signals (see Fig. 7 for labelling): (a) 2.01 (Me^{II} $\mathbf{8}^+$), 2.10 (Me $\mathbf{7}^+$), 2.20 (Me^{I} $\mathbf{8}^+$), (b) 5.96 (NH^{I} $\mathbf{8}^+$), 5.57 (NH^{II} $\mathbf{8}^+$), 4.43 (NH $\mathbf{7}^+$); (b) –9.90 (IrH $\mathbf{8}^+$), 5.87 (C^2H^{II} $\mathbf{8}^+$), 7.19 (C^6H^{I} $\mathbf{8}^+$); (c) 4.36 (CH^{cod} $\mathbf{7}^+$), 5.29 (C^dH $\mathbf{8}^+$), 4.01 (C^bH $\mathbf{8}^+$); d) 6.14 (C^3H^{II} $\mathbf{8}^+$), 6.59 (C^3H^{I} $\mathbf{8}^+$), 6.72 (C^3H $\mathbf{7}^+$), 6.96 (C^5H^{I} $\mathbf{8}^+$)].

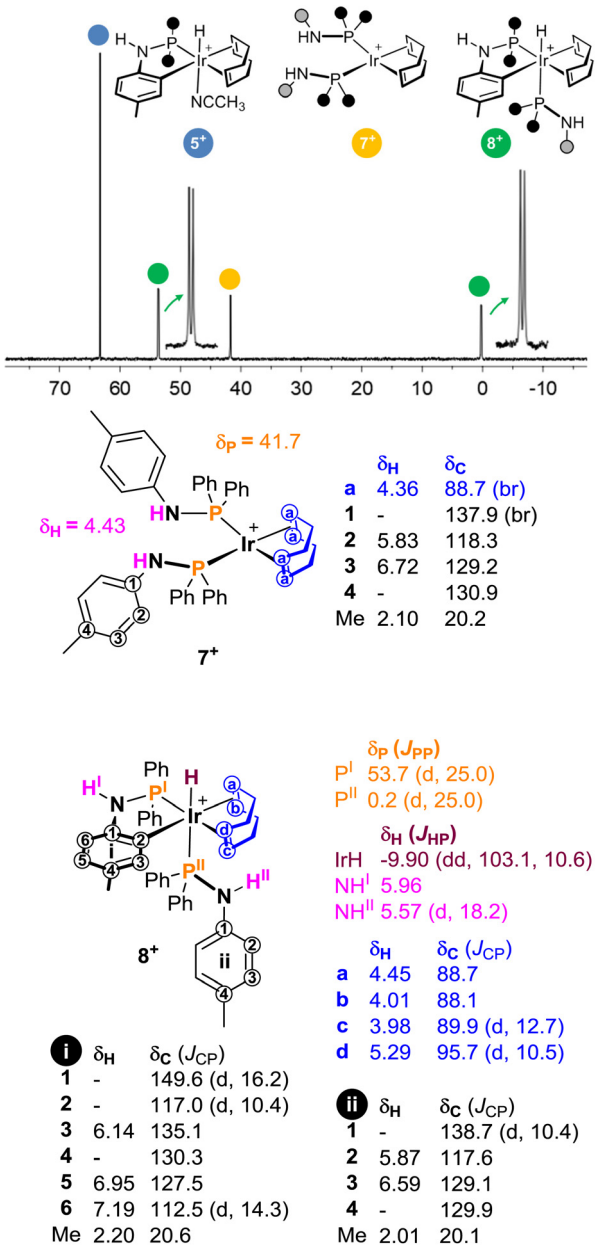

Fig. 7 (Top) $^{31}P\{^1H\}$ NMR of the CD_2Cl_2 solution resulting from the reaction of $[Ir(CH_3CN)_2(cod)][PF_6]$ and HNP (1 : 1) at 233 K, with the proposed assignment; (bottom) selected ^1H, $^{13}C\{^1H\}$ and $^{31}P\{^1H\}$ NMR data for $\mathbf{7}^+$ and $\mathbf{8}^+$ (δ are given in ppm, J in Hz).

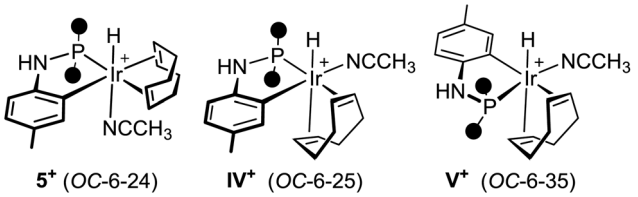

Fig. 8 Isomers of $[IrH\{\kappa^2C,P\text{-}NH(4\text{-}C_6H_3CH_3)PPh_2\}(cod)(CH_3CN)]^+$.

Open Access Article. Published on 25 July 2022. Downloaded on 1/21/2026 6:06:26 AM.
This article is licensed under a Creative Commons Attribution-NonCommercial 3.0 Unported Licence.

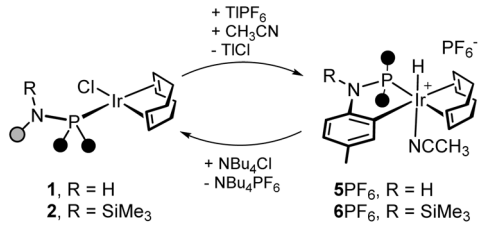

Scheme 8 Reversible Formation of $\mathbf{5}PF_6$ and $\mathbf{6}PF_6$.

the CH_3CN ligand and a severe distortion of the resulting square pyramidal structure (ΔG_{rel} = +20.6 kcal mol^{-1}).

Interestingly, the cyclometalation of the tolyl group can be reverted by reacting $\mathbf{5}^+$ or $\mathbf{6}^+$ with chloride (Scheme 8). Actually, the reaction of $\mathbf{5}PF_6$ or $\mathbf{6}PF_6$ with tetrabutylammonium chloride (1 : 1) cleanly and immediately affords **1** and **2**, respectively.** On the other hand, $\mathbf{5}PF_6$ and $\mathbf{6}PF_6$ were also obtained *via* chloride abstraction upon treating **1** and **2**, respectively, with $TlPF_6$ in CH_3CN (Scheme 8). On these grounds, the C–H oxidative addition to iridium in [IrX(RNP)(cod)]$^{n+}$ (X = Cl, n = 0; X = CH_3CN, n = 1, R = H, $SiMe_3$) is subtly controlled by the ancillary ligand X. Actually, it should be hampered by the chlorido ligand and facilitated when the acetonitrile ligand is present, instead. With this in mind, the Gibbs free energy profiles of the cyclometalation reaction for **1** and [Ir(cod)(HNP)(CH_3CN)]$^+$ ($\mathbf{III}^+$) were explored by means of DFT calculations (Fig. 9). Despite the fact that the activation barriers are easily accessible at room temperature for both **1** (*cf.* **TS_1-VI**, ΔG_{act} = +17.5 kcal mol^{-1}) and $\mathbf{III}^+$ (*cf.* **TS_III$^+$-5$^+$**, ΔG_{act} = +11.5 kcal mol^{-1}), the relative stability of the hydrido derivative *vs.* the related square complex are different. As a matter of fact, in agreement with the observed outcome of the reactions given in Scheme 8, the putative hydrido complex [IrHCl{κ^2*C*,*P*-NH(4-$C_6H_3CH_3$)PPh_2}(cod)] (**VI**) is less stable than the parent square planar complex [IrCl(HNP)(cod)] (**1**), whereas [IrH{κ^2*C*,*P*-NH(4-$C_6H_3CH_3$)PPh_2}(cod)(CH_3CN)]$^+$ ($\mathbf{5}^+$) is more stable than [Ir(cod)(HNP)(CH_3CN)]$^+$ ($\mathbf{III}^+$, Fig. 9), which indicates that switching from X = CH_3CN to X = Cl$^-$ in [IrX(RNP)(cod)]$^{n+}$ makes the oxidative addition unfavourable.

For the sake of comparison, the energy profile of the reaction $\mathbf{7}^+ \rightarrow \mathbf{8}^+$ was also calculated (Fig. SI46 ESI†) confirming that this transformation is a fast equilibrium under the explored reaction conditions.

In view of the reaction sequence discussed in Scheme 7, the reaction of $\mathbf{5}^+$ with HNP (1 : 1) was carried out aiming at preparing $\mathbf{8}^+$. Surprisingly, on a preparative scale an inseparable mixture of products was obtained, and monitoring the reaction at 233 K evidenced the formation of a mixture of products mainly containing $\mathbf{8}^+$ and a new thermally unstable product, which was independently prepared at 233 K and identified

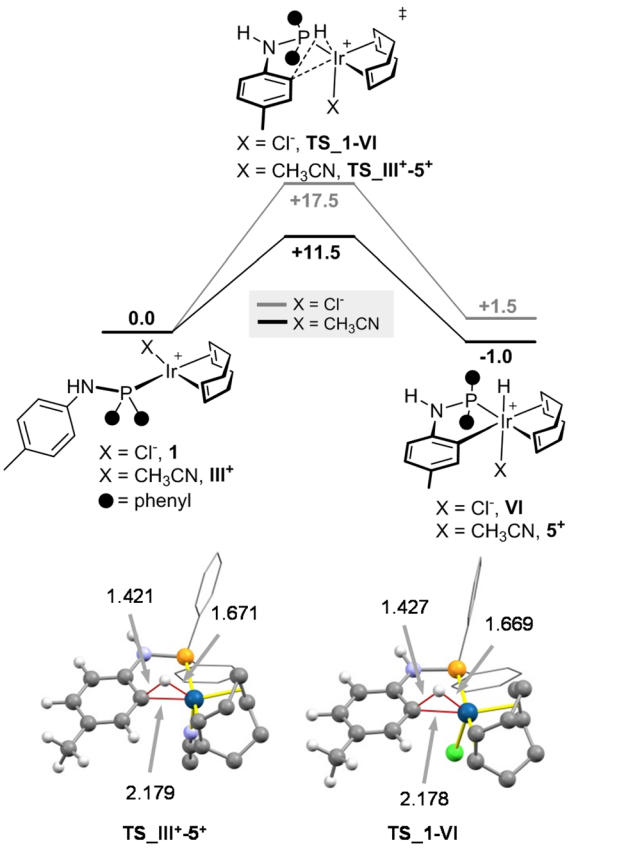

Fig. 9 (Top) Gibbs free energy profile for the formation of [IrHX{κ^2*C*,*P*-HN(4-$C_6H_3CH_3$)PPh_2}(cod)]$^{n+}$ (X = CH_3CN, $\mathbf{5}^+$; Cl$^-$, **II**) along with the calculated Gibbs free energies (kcal mol^{-1}, M06/def2tzvp//B3PW91-GD3BJ/def2svp, CH_2Cl_2, 298 K, 1 atm). (bottom) View of **TS_I$^+$-5$^+$** and **TS_1-II** along with selected interatomic distances (Å). For clarity, most hydrogen atoms have been omitted and phenyl groups are shown in a wireframe style. Blue, iridium; gray, carbon; orange, phosphorus; green, chlorine; violet, nitrogen; white, hydrogen.

in situ as [Ir$(HNP)_3$(cod)]$^+$ ($\mathbf{9}^+$).†† In addition, when the reaction mixture was heated up to room temperature, $\mathbf{8}^+$ disappeared and a mixture of products was obtained including, among others, hydrido derivatives containing three HNP ligands. This evidence suggests that the outcome of the reaction of $\mathbf{5}^+$ with HNP is spoiled by the reversibility of the CH oxidative addition as well as by the formation of substitution products containing up to three HNP ligands per iridium.

A CD_2Cl_2 solution (0.5 mL) of $\mathbf{5}PF_6$ or $\mathbf{6}PF_6$ (0.021 mmol) was added with $[NBu_4]Cl$ (0.021 mmol). Soon after mixing, the clean formation of **1 and **2**, respectively, was observed ($^{31}P\{^1H\}$ NMR spectroscopy).

††[Ir$(HNP)_3$(cod)]$^+$ ($\mathbf{9}^+$) was prepared by reaction of HNP and [Ir(cod)$(CH_3CN)_2$][PF_6] (Ir : HNP = 1 : 3) at 223 K in CD_2Cl_2 as a thermally unstable compound and was spectroscopically identified *in situ* in the presence of about 20 mol% of unidentified by-products. At 233 K, its $^{31}P\{^1H\}$ NMR spectrum shows a broad signal at 18.5 ppm ($\Delta\nu_{1/2}$ = 26 Hz). Accordingly, one ^1H singlet is observed at 2.19 ppm for the methyl moiety of the tolyl groups and one broad ^1H signal at 3.41 ppm is observed for the cod HC=CH moieties. On this ground, [Ir$(HNP)_3$(cod)]$^+$ is likely to undergo a fluxional process exchanging the three HNP ligands as well as averaging the coordinated cod ligand. In this regard, similar to **3**, an equilibrium between square pyramidal (*SPY*-3-12) and trigonal bipyramidal structures (*TBPY*-5-12) may account for the observed solution behaviour.

This journal is © The Royal Society of Chemistry 2022

Open Access Article. Published on 25 July 2022. Downloaded on 1/21/2026 6:06:26 AM.
This article is licensed under a Creative Commons Attribution-NonCommercial 3.0 Unported Licence.

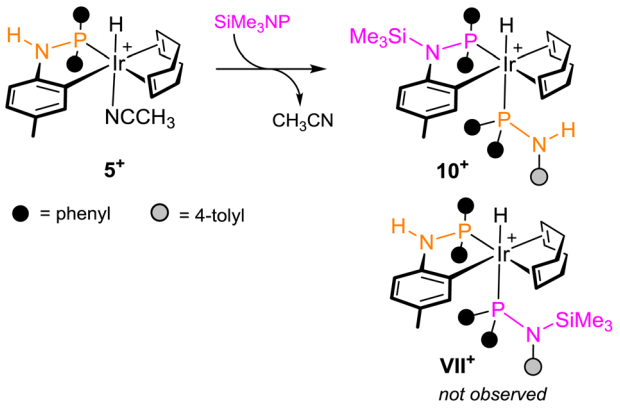

Scheme 9 Reaction of 5^+ with $SiMe_3NP$.

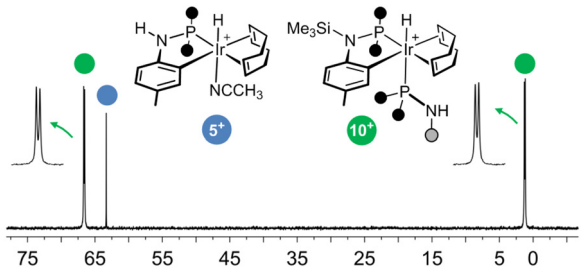

Fig. 10 $^{31}P\{^1H\}$ NMR spectrum of 10^+ (prepared *in situ*) with traces of residual 5^+ (6 mol% approx.).

Also, the reaction of 5^+ with $SiMe_3NP$ was carried out, envisioning that the higher steric hindrance of $SiMe_3NP$ could prevent the formation of unwanted products (Scheme 9). As a matter of fact, this reaction smoothly takes place at 233 K in 6 h rendering the unexpected compound 10^+ (along with residual amounts of unreacted 5^+, Fig. 10). Notably, the formation of 10^+ (instead of VII^+, Scheme 9) indicates that 5^+ does not simply exchange the CH_3CN ligand with the incoming $SiMe_3NP$, but also that, at some point, the CH reductive elimination rendering HNP and the following CH oxidative addition at $SiMe_3NP$ take place. The ^1H and $^{13}C\{^1H\}$ signals assigned to the tolyl groups (see ESI, Fig. SI7†) confirm the presence of the $[Ir\{\kappa^2C,P\text{-}SiMe_3N(4\text{-}C_6H_3CH_3)P\}]$ moiety along with the κP HNP ligand. Also the $^2J_{HP}$ coupling constants (105.5, 12.4 Hz) of the ^1H signal at −10.18 ppm of the Ir–H moiety and the $^2J_{PP}$ constant (22.2 Hz) support the structure proposed for 10^+.

Finally, for the sake of comparison, the relative stability of 10^+ and of the expected isomer VII^+ was calculated by DFT methods showing that 10^+ is 31.5 kcal mol^{-1} more stable than VII^+, reasonably because of the high steric congestion that exists between the trimethylsilyl group and the metalated tolyl group (Fig. 11). In our hands, any attempt to isolate 10^+ was unsuccessful due to its limited thermal stability.

Reactivity with $[Ir(CH_3CN)_2(coe)_2][PF_6]$. The reaction of $[Ir(CH_3CN)_2(coe)_2][PF_6]$ with $SiMe_3NP$ or HNP was carried out, a different outcome being observed in each case (coe = cyclooctene, Scheme 10). Indeed, $[Ir(CH_3CN)_2(coe)_2][PF_6]$ reacts with $SiMe_3NP$ (1 : 2 molar ratio) affording the square planar complex $[Ir(CH_3CN)_2(SiMe_3NP)_2]^+$ (11^+), isolated as the hexafluorophosphate salt, as a result of the substitution of the coe ligands. In agreement with the square planar geometry at the metal centre, one $^{31}P\{^1H\}$ singlet at 61.9 ppm is observed for the two equivalent phosphorus atoms, along with two ^1H singlets at 1.42 and 0.03 ppm for the equivalent acetonitrile ligands and the trimethyl silyl groups, respectively. On the other hand, the reaction of $[Ir(CH_3CN)_2(coe)_2][PF_6]$ with HNP

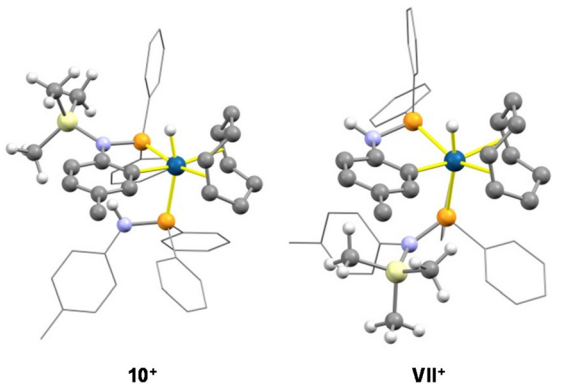

Fig. 11 Calculated structures of 10^+ and VII^+ (B3PW91-GD3BJ/def2svp). For clarity, most hydrogen atoms are omitted and most tolyl and phenyl groups are shown in a wireframe style. Blue, iridium; gray, carbon; orange, phosphorus; yellow, silicon; violet, nitrogen; white, hydrogen. Blue, iridium; gray, carbon; orange, phosphorus; yellow, silicon; violet, nitrogen; white, hydrogen.

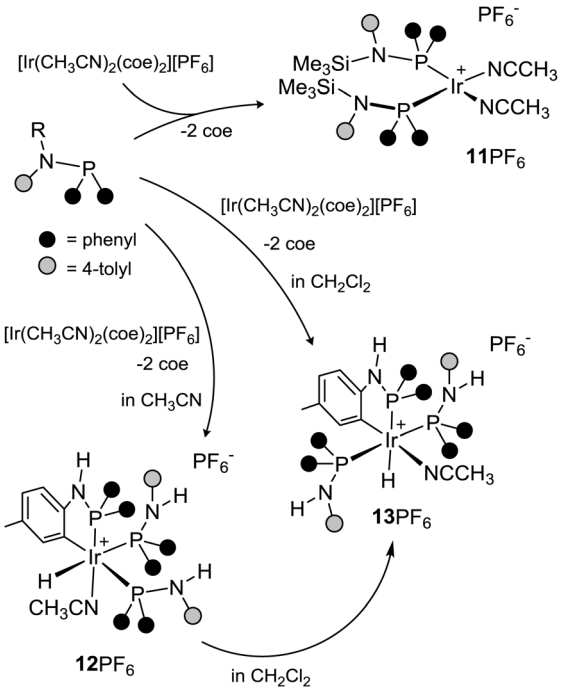

Scheme 10 Reaction of $[Ir(CH_3CN)_2(coe)_2]^+$ with HNP or $SiMe_3NP$.

Open Access Article. Published on 25 July 2022. Downloaded on 1/21/2026 6:06:26 AM.
This article is licensed under a Creative Commons Attribution-NonCommercial 3.0 Unported Licence.

entails the intramolecular C–H oxidative addition to iridium, yielding the iridium(III) hydrido isomers **12**$^+$ (*OC*-6-35) and **13**$^+$ (*OC*-6-52) of formula $[IrH\{\kappa^2C,P\text{-}NH(4\text{-}C_6H_3CH_3)PPh_2\}(HNP)_2(CH_3CN)]^+$, isolated as the hexafluorophosphate salts when the reaction was carried out in CH_3CN or CH_2Cl_2, respectively (Scheme 10). More specifically, in CD_2Cl_2, **12**$^+$ is the kinetic product observed in the first place ($^{31}P\{^1H\}$NMR), whereas **13**$^+$ is finally obtained as the thermodynamic product. On the contrary, in CD_3CN, only **12**$^+$ forms, **13**$^+$ being not observed ($^{31}P\{^1H\}$ NMR). Accordingly, when a CD_2Cl_2 solution of **12**$^+$ was allowed to stand at room temperature for 12 h, the clean conversion of **12**$^+$ into **13**$^+$ takes place (ESI, Fig. SI45†).

The solid state structure of **12**PF_6 was determined by means of single crystal X-ray diffraction measurements (Fig. 12). The asymmetric unit of **12**PF_6 contains two crystallographically independent pairs of the ions *OC*-6-35-$[IrH\{\kappa^2C,P\text{-}NH(4\text{-}C_6H_3CH_3)PPh_2\}(HNP)_2(CH_3CN)]^+$ and PF_6^- (ESI, Fig. S12†). Similar to **6**$^+$, **12**$^+$ contains a stereogenic metal centre, and the cations of the asymmetric unit are chemically equivalent, but exhibit different configurations at the metal centre. When comparing bond lengths and angles, similar values are observed for the two enantiomers. Therefore, for the sake of brevity, only the crystal structure of the enantiomer *C* is discussed in detail (Fig. 12). An octahedral environment is observed at the metal centre with a facial disposition of the three phosphorus atoms P1, P2 and P3. The remaining coordination sites are occupied by the hydrido ligand H1m (*trans* to P3), the acetonitrile ligand (*trans* to P1) and the carbon atom C14 of the metalated tolyl group (*trans* to P2). Similar to **6**$^+$, the

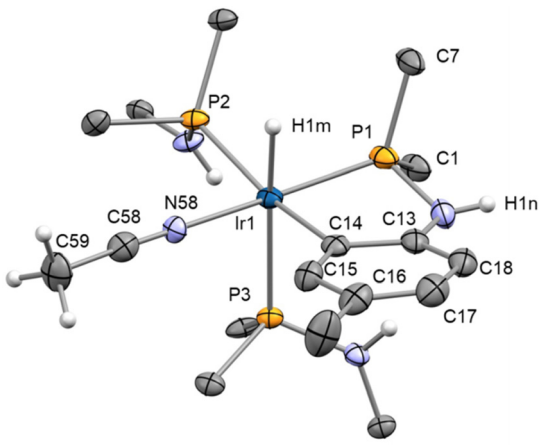

Fig. 12 ORTEP plot of *C*$_{Rh}$-*OC*-6-35-$[IrH\{\kappa^2C,P\text{-}HN(4\text{-}C_6H_3CH_3)PPh_2\}(HNP)_2(CH_3CN)][PF_6]$ (*C*$_{Rh}$-**12**PF_6). For clarity most hydrogen are omitted and only *ipso* carbon atoms of the phenyl and tolyl groups are shown. Thermal ellipsoids are at 50% probability. Selected bond lengths (Å) and angles (°) are: N58–Ir1 2.062(3), P1–Ir1 2.2484(10), P2–Ir1 2.3387(10), P3–Ir1 2.4027(9), Ir1–H1m 1.54(4), C14–Ir1 2.103(4), C13–C14 1.407(5), C13–N1 1.412(5), N1–P1 1.680(4), C14–Ir1–P1 81.14(11), P1–Ir1–H1m 83.1(19), C14–Ir1–H1m 84.1(18), P3–Ir1–H1m 172.6(19), P1–Ir1–P2 98.90(4), P1–Ir1–P3 97.96(3), P2–Ir1–P3 105.03(3), N58–Ir1–P1 166.85 (9).

$[Ir\{\kappa^2C,P\text{-}NH(4\text{-}C_6H_3CH_3)P\}]$ moiety of **12**$^+$ is planar and the bond lengths N1–P1 [1.680(4) Å] and C13–N1 [1.412(5) Å] indicate a nitrogen–phosphorus back-donation with a nitrogen–carbon single bond.

Based on the NMR spectra of **12**$^+$, its solid state structure should be maintained in solution. Specifically, three $^{31}P\{^1H\}$ signals are observed at 49.8 (P^1), 19.8 (P^2) and 11.2 ppm (P^3) with $^2J_{PP}$ coupling constants (16.9, 11.5 Hz) indicating a mutually *cis* disposition. Accordingly, three ^1H signals are observed for the non-equivalent NH groups (δ_H 6.28, HNP^1; 5.17, HNP^2; 4.64 ppm, HNP^3). The ^1H signal of the hydrido ligand at −11.83 ppm is observed as a doublet of triplets with $^2J_{HP}$ constants (150.5, 16.2 Hz) underpinning the presence of two phosphorus atoms at *cis* positions (P^1 and P^2) and one (P^3) at the *trans* position. The ^1H and $^{13}C\{^1H\}$ signals assigned to the tolyl group are similar to those observed for **6**$^+$, thus confirming its metalation (see ESI Fig. SI8† for selected ^1H, $^{13}C\{^1H\}$ and $^{31}P\{^1H\}$ data and the proposed assignment).

Also, the solution structure of **13**$^+$ was established by means of multinuclear NMR spectroscopy. Relevant for the solution structure elucidation, the $^{31}P\{^1H\}$ spectrum contains two signals at 43.4 and 19.7 ppm assigned to the metalated $Ir\{\kappa^2C,P\text{-}NH(4\text{-}C_6H_3CH_3)P\}$ moiety and the equivalent HNP ligands, respectively. Accordingly, two ^1H signals are observed for the NH moieties at 5.57 (1H) and 5.18 ppm (2H). The hydrido ligand lies *trans* to the phosphorus atom of the metalated HNP ligand originating a ^1H doublet of triplets at −9.86 ppm ($^2J_{HP}$ = 133.0, 18.6 Hz). Like for **12**$^+$, the ^1H and $^{13}C\{^1H\}$ signals assigned the tolyl groups confirm the presence of one metalated tolyl group (see ESI Fig. SI8†).

As for the formation of **12**$^+$ and **13**$^+$, DFT calculations were performed in order to shed light on the underlying reaction sequence. Provided that $[Ir(CH_3CN)_2(SiMe_3NP)_2]^+$ (**11**$^+$) forms upon reaction of $[Ir(CH_3CN)_2(coe)_2]^+$ with $SiMe_3NP$, the related complex $[Ir(CH_3CN)_2(HNP)_2]^+$ (**VIII**$^+$) is assumed as the starting point for the formation of **12**$^+$ (Fig. 13A). Two routes leading from **VIII**$^+$ to **12**$^+$ can be envisioned. On one hand (Fig. 13A, red arrows), the oxidative addition of the CH bond to iridium in **III**$^+$ leads to the iridium(III) hydrido derivatives **IX**$^+$ or **X**$^+$, depending on the regiochemistry of the CH oxidative addition. The barriers for the formation of **IX**$^+$ (**TS_VIII**$^+$**-IX**$^+$, +16.6 kcal mol^{-1}) and **X**$^+$ (**TS_VIII**$^+$**-X**$^+$,‡‡ $\Delta E_{act} \approx$ +16.7 kcal mol^{-1}) are accessible at room temperature. On their turn, **IX**$^+$ or **X**$^+$ might undergo a substitution reaction exchanging CH_3CN with HNP. Indeed, the CH_3CN ligand *trans* to carbon atom (**IX**$^+$) or hydrido ligand (**X**$^+$) are expected to be labile and prone to being replaced by the incoming HNP ligand, thus rendering **12**$^+$. On the other hand (Fig. 13A, blue arrows), **VIII**$^+$ might convert into the square planar intermediate **XII**$^+$ *via* a presum-

‡‡The transition state **TS_VIII**$^+$**-X**$^+$ could not be located on the PES. So, the reported activation barrier was estimated ($\Delta E_{act} \approx$ +16.7 kcal·mol^{-1}) scanning the C–H coordinate of the carbon–hydrogen bond undergoing oxidative addition to the iridium centre.

This journal is © The Royal Society of Chemistry 2022

Open Access Article. Published on 25 July 2022. Downloaded on 1/21/2026 6:06:26 AM.
This article is licensed under a Creative Commons Attribution-NonCommercial 3.0 Unported Licence.

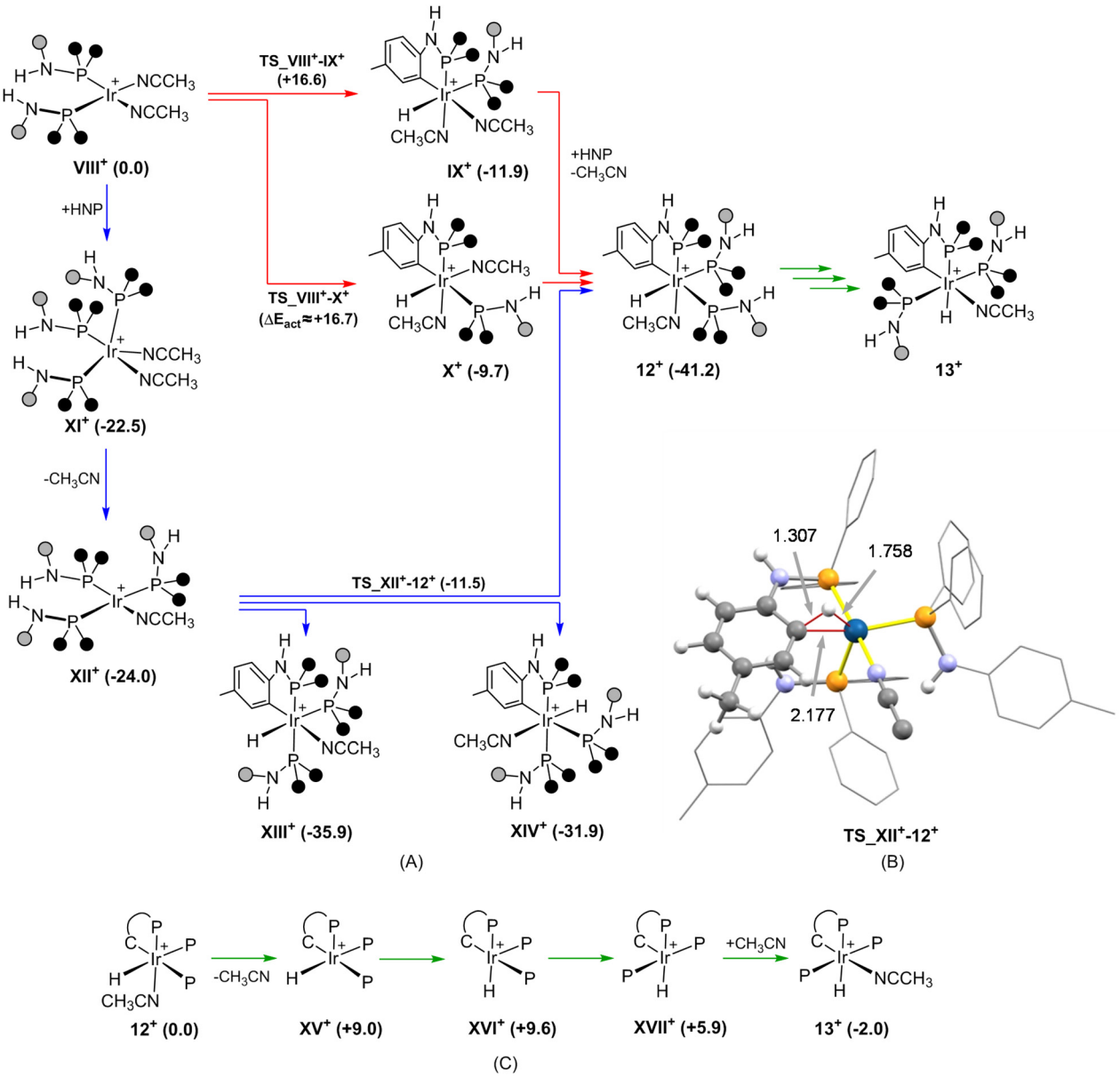

Fig. 13 (A) Reaction sequences for the formation of $\mathbf{12}^+$ and $\mathbf{13}^+$ with the relative Gibbs free energy (kcal mol^{-1}, B3PW91-GD3BJ/def2svp) of the proposed intermediates and transition states. (B) Calculated structure for the transition state $\mathbf{TS_XII}^+\mathbf{-11}^+$ along with selected interatomic distances (Å, B3PW91-GD3BJ/def2svp). For clarity, most hydrogen atoms are omitted and phenyl and selected tolyl groups are shown in a wireframe style. (C) Proposed reaction sequence for the isomerization of $\mathbf{12}^+$ to $\mathbf{13}^+$ (M06/def2tzvp//B3PW91-GD3BJ/def2svp).

ably barrierless, exergonic associative mechanism§§ going through the pentacoordinate derivative $\mathbf{XI}^+$. Subsequently, $\mathbf{XII}^+$ should undergo the intramolecular CH oxidative addition and, depending on the implied tolyl group and on the regiochemistry of the CH oxidative addition itself, $\mathbf{12}^+$, $\mathbf{XIII}^+$ or $\mathbf{XIV}^+$ might form. Notably, both $\mathbf{XIII}^+$ and $\mathbf{XIV}^+$ are calculated to be less stable than $\mathbf{12}^+$, in agreement with the fact that neither of them was obtained. Also the transition state $\mathbf{TS_XII}^+\mathbf{-12}^+$ (Fig. 13B) leading from $\mathbf{XII}^+$ to $\mathbf{12}^+$ was calculated to be accessible at room temperature (Fig. 13A, ΔG_{act} = +12.5 kcal mol^{-1}). With this in mind, both routes are accessible under experimental conditions. Nonetheless, from an energetic point of view, starting from $\mathbf{VIII}^+$, the route *via* $\mathbf{IX}^+$ and $\mathbf{X}^+$ (red arrows) goes up to approx. +17 kcal mol^{-1} (corresponding to the transition states $\mathbf{TS_VIII}^+\mathbf{-IX}^+$ and $\mathbf{TS_VIII}^+\mathbf{-X}^+$) and then downhill to $\mathbf{12}^+$, whereas the route *via* $\mathbf{XI}^+$ (blue arrows) goes through two exergonic initial steps ($\mathbf{VIII}^+ \rightarrow \mathbf{IX}^+$, ΔG = −22.5 kcal mol^{-1}; $\mathbf{IX}^+ \rightarrow \mathbf{X}^+$, ΔG = −1.5 kcal mol^{-1}) followed by the CH oxidative addition rendering $\mathbf{12}^+$, which is feasible under experimental

§§ The dissociative route was also considered and finally discarded since the tricoordinate intermediate $[Ir(HNP)_2(CH_3CN)]^+$ was calculated to lie at +14.5 kcal mol^{-1} *vs.* $\mathbf{VIII}^+$.

Open Access Article. Published on 25 July 2022. Downloaded on 1/21/2026 6:06:26 AM.
This article is licensed under a Creative Commons Attribution-NonCommercial 3.0 Unported Licence.

Table 1 Selected experimental data for the dehydrogenation of formic acid catalysed by **1–3**, **5**PF_6, **6**PF_6, **11**PF_6 and **13**PF_6 [a]

Entry	Catalyst	Cat. mol%	Base	Base mol%	Conv.%[b], time	$TOF_{1\ min}$ [c] (h^{-1})
1	**1**	1%	NaHCOO	10%	38%, 40 min	400
2	**2**	1%	NaHCOO	10%	68%, 40 min	240
3	**3**	1%	NaHCOO	10%	92%, 18 min	1700
4	**5**PF_6	1%	NaHCOO	10%	37%, 40 min	240
5	**6**PF_6	1%	NaHCOO	10%	30%, 40 min	150
6	**11**PF_6	1%	NaHCOO	10%	94%, 35 min	500
7	**13**PF_6	1%	NaHCOO	10%	95%, 18 min	680
8	**3**	1%	NaHCOO	50%	97%, 18 min	1640
9	**3**	5%	NaHCOO	50%	99%, 0.8 min	2330
10	**3**	1%	NEt_3	10%	96%, 25 min	1000
11	**3**	5%	NEt_3	50%	98%, 2 min	900

[a] Reaction conditions: 20 mL of DMF, 20 μL of HCOOH (0.529 mmol), NaHCOO or NEt_3 (10 or 50 mol%), iridium catalyst (1 or 5 mol%), 353 K. [b] Based on the pressure of the resulting gas mixture. [c] $TOF_{1\ min}$ is calculated as TON at 1 min divided by 1 min.

conditions (ΔG_{act} = +12.5 kcal mol^{-1}, **TS_XII**$^+$**-12**$^+$ *vs.* **XII**$^+$). As a result, even if the route *via* **IX**$^+$ and **X**$^+$ (red arrows) is viable, the reaction sequence going through **XII**$^+$ (blue arrows) is more favourable and should be operative under experimental conditions.

As far as the formation of **13**$^+$ is concerned, the meridional disposition of the phosphorus and carbon atoms and of the hydrido ligand within the IrH{κ^2*C*,*P*-HN(4-$C_6H_3CH_3$)PPh_2} moiety rules out that **13**$^+$ might result from the straightforward CH oxidative addition to iridium.¶¶

Thus, the transformation of **12**$^+$ into **13**$^+$ should be the result of a genuine isomerization process which alters the disposition of the ligands at the metal centre, and more than likely is triggered by the dissociation of CH_3CN when **12**$^+$ is dissolved in CH_2Cl_2. On this basis, Fig. 13C depicts a plausible reaction sequence (green arrows) for the conversion of **12**$^+$ into **13**$^+$ along with the calculated relative Gibbs free energy of the proposed intermediates. In the first place, the dissociation of CH_3CN from **12**$^+$ renders the pentacoordinated iridium complex **XV**$^+$ which stepwise isomerise to **XVII**$^+$ *via* **XVI**$^+$. Finally, **13**$^+$ forms upon reaction of **XVII**$^+$ with CH_3CN.

Catalytic dehydrogenation of formic acid

The iridium(I) derivatives **1–3** and **11**PF_6, and the iridium(III) compounds **5**PF_6, **6**PF_6, and **13**PF_6 were tested as catalysts for formic acid dehydrogenation. Preliminary catalytic tests (1 mol% catalyst, 10 mol% NaHCOO, in DMF at 80 °C) revealed that IrCl(HNP)$_2$(cod) (**3**) is by far the most active catalyst (Table 1, entries 1–7) reaching $TOF_{1\ min}$ of about 1700 h^{-1} and complete conversion to H_2 and CO_2 after 18 min, CO not being observed in the resulting gas mixture (IR). In this regard, these preliminary data point out that the presence of two aminophosphano ligands, each one with an available NH group, may be responsible for the good catalytic performance of **3**. When using 1 mol% of **3** as a catalyst, increasing the amount of sodium formate up to 50 mol% does not increase the activity of the catalyst (Table 1, entry 8). Notably, when 5 mol% of **3** along with 50 mol% of sodium formate was used a short induction time was clearly observed (Fig. 14) and a $TOF_{1\ min}$ of about 2300 h^{-1} (Table 1, entry 9) was reached, which indicates that its activity is similar to that reported for the iridium complexes [IrCp*(H_2O)(2,2′-bipyridine-4,4′-diol)]$^{2+}$ (ref. 6*k*) and [IrCp*Cl{1,2-$(NH)_2C_6H_{10}$}]$^+$.[6g] Also, at a 5 mol% catalyst loading and 50 mol% of sodium formate, **3** showed a decreasing activity upon consecutively adding formic acid, without any induction period (**C–F**, Fig. 14). When triethyl-

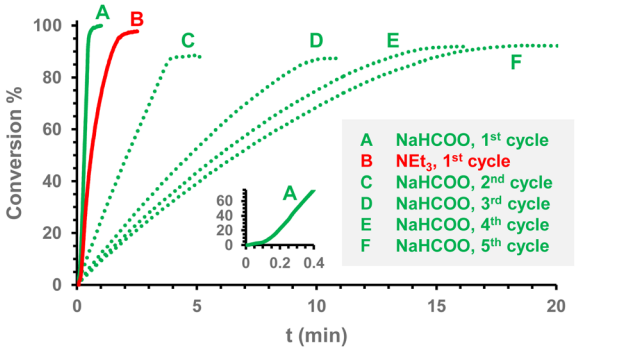

Fig. 14 Conversion *vs.* time profiles for the formic acid dehydrogenation catalysed by **3** (5% catalyst, 50% base, DMF, 80 °C).

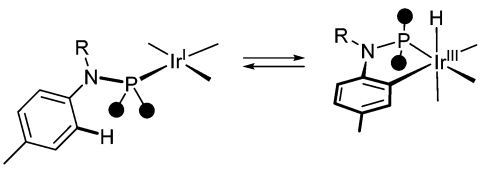

Scheme 11 Reversible CH oxidative addition to iridium.

¶¶Actually, the meridional disposition of the hydrido ligand, the phosphorus and carbon (tolyl) atoms within the IrH{κ^2*C*,*P*-HN(4-$C_6H_3CH_3$)PPh_2} moiety may only result from a parallel arrangement of the reacting C–H bond and the iridium–phosphorus bond, which is incompatible with the topology of the Ir(HNP) fragment. In other words, the tether of the tolyl group to the phosphorus atom restricts the reacting C–H bond to lying perpendicular to the iridium–phosphorus bond (of the aminophosphano ligand undergoing the CH oxidative addition), which may uniquely affords a mutually *cis* disposition of the hydrido ligand, and the phosphorus and carbon (tolyl) atoms (*cf.* **TS_XII**$^+$**-12**$^+$, Fig. 13B).

This journal is © The Royal Society of Chemistry 2022

Open Access Article. Published on 25 July 2022. Downloaded on 1/21/2026 6:06:26 AM. This article is licensed under a Creative Commons Attribution-NonCommercial 3.0 Unported Licence.

amine was used as a base instead of sodium formate (Table 1, entries 10 and 11), a lower activity was observed for **3** ($TOF_{1\ min}$ 1000 h^{-1}, Fig. 14).

Conclusions

Monodentate aminophosphanes HNP [NH(4-tolyl)PPh_2] and $SiMe_3$NP [$SiMe_3$N(4-tolyl)PPh_2] react with iridium(I) precursors affording a varied family of iridium(I) and cyclometalated iridium(III) complexes, exhibiting κP or κ^2C,P coordination modes. The tetra- or pentacoordinate iridium(I) complexes [IrCl(κ*P*-RNP)$_n$(cod)] (R = H, n = 1, 2; R = $SiMe_3$, n = 1) result from bridge splitting at [Ir(μ-Cl)(cod)]$_2$, the steric hindrance of the incoming aminophosphane being decisive in the outcome of the reaction. On the other hand, octahedral iridium(III) complexes can also be obtained as a result of the intramolecular CH oxidative addition of the C^2–H bond of the tolyl substituent of both HNP and $SiMe_3$NP to iridium(I) rendering the [IrH{κ^2C,P-RN(4-$C_6H_3CH_3$)P}] moiety. The calculated activation barrier of the CH oxidative addition is relatively small and the related CH reductive elimination can be smoothly triggered (Scheme 11). Unexpectedly, complex reaction sequences have been observed as a consequence of the reversibility of the CH oxidative addition and/or competing substitution reactions.

Both iridium(I) and iridium(III) derivatives catalyze the dehydrogenation of formic acid in DMF, the iridium(I) compound [IrCl(HNP)$_2$(cod)] being the most active species. A detailed study on the reaction mechanism operative in the dehydrogenation of formic acid catalysed by **3** is under run in order to elucidate the role of the NH groups as well as the influence of the structure of the iridium-aminophosphane platform on the observed catalytic activity.

Experimental

General section

All the operations were carried out using standard Schlenk tube techniques under an atmosphere of pre-purified argon or in a Braun glove-box under argon. Organic solvents were dried by standard procedures and distilled under argon or obtained oxygen- and water-free from a Solvent Purification System (Innovative Technologies). The compounds NH(4-tolyl)PPh_2 (HNP),[8] [Ir(μ-Cl)(cod)]$_2$,[14] and [Ir(CH_3CN)$_2$(cod)][PF_6][15] were prepared according to the literature. [Ir(CH_3CN)$_2$(coe)$_2$][PF_6] was obtained as a spectroscopically pure solid following a procedure similar to that reported by Milstein for [Ir(acetone)$_2$(coe)$_2$][PF_6].[16] NMR spectra were recorded with Bruker spectrometers (AV300, AV400, and AV500) and are referred to $SiMe_4$ (^{1}H, ^{13}C{^{1}H}) and H_3PO_4 (^{31}P{^{1}H}). The proposed ^{1}H, ^{13}C{^{1}H}, and ^{31}P{^{1}H} assignment relies on the combined analysis of 1D [^{1}H, ^{1}H{^{31}P}, ^{13}C{^{1}H}-apt, ^{31}P{^{1}H}] and 2D NMR spectra (^{1}H–^{1}H COSY, ^{1}H–^{1}H NOESY, ^{1}H–^{13}C HSQC, ^{1}H–^{13}C HMBC, ^{1}H–^{31}P HMBC). For **5**PF_6 and **6**PF_6, olefinic carbon and hydrogen atoms are labelled as "up" or "down" if they point towards the hydride or if they do not, respectively, and as "*trans*" or "*cis*" if the HC=CH moiety lies *trans* to phosphorus or *cis* to it, respectively. For **12**PF_6 and **13**PF_6, labels P^1, P^2, and P^3 are used for non-equivalent phosphorus atoms, and, accordingly, superscript labels "tol-P1/2/3" and "PhP1/2/3" are used for hydrogen and carbon atoms belonging to the tolyl and phenyl groups attached/linked to the phosphorus atom P^1/P^2/P^3. As for the reaction monitored by NMR spectroscopy at low temperature, the working temperature of 233 K was chosen in order to avoid the precipitation of reactants and/or products. C, H, and N analyses were carried out on a Perkin-Elmer 2400 CHNS/O analyzer. Infrared spectra were recorded on a Thermo Nicolet Avatar 360 FT-IT spectrometer on CH_2Cl_2 solutions using KBr windows (1 mm path).

Synthesis of $SiMe_3$N(4-tolyl)PPh_2 ($SiMe_3$NP)

A solution of NH(4-tolyl)PPh_2 (2.43 g, 8.34 mmol, 291.33 g mol^{-1}) in THF (10 mL) and toluene (25 mL) at 198 K was treated with *n*-BuLi (1.6 M in hexane, 5.2 mL, 8.3 mmol). The mixture was allowed to warm up to room temperature (1 h) and $SiMe_3Cl$ (1.06 mL, 8.35 mmol, 0.856 g mL^{-1}, 108.64 g mol^{-1}) was added. After stirring overnight at room temperature, the suspension was heated at 333 K for 3 h. All the volatiles were removed *in vacuo* and the residue was extracted with CH_2Cl_2. The liquid phase was evaporated up to 3 mL and added with hexane (10 mL), affording the precipitation of a colourless solid, which was filtered off and washed with diethyl ether, dried *in vacuo*, and finally identified as $SiMe_3$N(4-tolyl)PPh_2 (1.61 g, 53% yield). Found: C 73.01, H 6.99, N 3.78. Calcd for $C_{22}H_{26}NPSi$ (363.51 g mol^{-1}): C 72.69, H 7.21, N 3.85. ^{1}H NMR (C_6D_6, 298 K): δ_H 7.66–7.52 (4H, *o*-PPh), 7.23–7.14 (6H tot; 4H *m*-PPh, 2H *p*-PPh), 6.75 (d, 2H, $^3J_{HH}$ = 8.8 Hz, C^3H^{tol}), 6.73 (d, 2H, $^3J_{HH}$ = 8.8 Hz, C^2H^{tol}), 2.07 (s, 3H, CH_3^{tol}), 0.47 (d, 9H, $^3J_{HP}$ = 1.0 Hz, $SiCH_3$). ^{13}C{^{1}H} NMR (C_6D_6, 298 K): δ_C 143.4 (d, $^2J_{CP}$ = 8.0 Hz, $C^{1,\ tol}$), 140.7 (d, $^1J_{CP}$ = 17.7 Hz, $C^{1,\ PhP}$), 134.7 ($C^{4,\ tol}$), 134.2 (d, $^2J_{CP}$ = 21.1 Hz, $C^{2,\ PhP}$), 130.9 (d, $^3J_{CP}$ = 1.3 Hz, $C^{2,\ tol}$), 129.6 ($C^{3,\ tol}$), 129.3 ($C^{4,\ PhP}$ $C^{3,\ tol}$), 128.7 (d, $^3J_{CP}$ = 5.9 Hz, $C^{3,\ PhP}$), 21.3 (CH_3^{tol}), 2.2 (d, $^3J_{CP}$ = 8.4 Hz, $SiCH_3$), ^{31}P{^{1}H} NMR (C_6D_6, 298 K): δ_P 50.5 (s).

Synthesis of [IrCl(HNP)(cod)] (1). A toluene solution (10 mL) of [Ir(μ-Cl)(cod)]$_2$ (315 mg, 0.469 mmol, 671.70 g mol^{-1}) was added with HNP (137 mg, 0.470 mmol, 291.33 g mol^{-1}) affording a deep orange solution. After 1 h stirring at room temperature, the solution was evaporated *in vacuo* up to approx. 5 mL and added with 20 mL of hexane. The resulting suspension was filtered, the solid washed with hexane (2 × 5 mL), dried *in vacuo* and finally identified as [IrCl(HNP)(cod)] (241 mg, 82% yield). Found: C 51.95, H 4.75, N 2.15. Calcd for $C_{27}H_{30}ClIrNP$ (627.18 g mol^{-1}): C 51.71, H 4.82, N 2.23. ^{1}H NMR (C_6D_6, 298 K): δ_H 8.01 (ddd, 4H, $^3J_{HP}$ = 10.9 Hz, $^3J_{HH}$ = 8.0 Hz, $^3J_{HH}$ = 1.6 Hz, *o*-PPh), 7.72 (d, $^2J_{HP}$ = 13.1 Hz, 1H, NH), 7.21–7.04 (6H tot; 4H, *m*-PPh; 2H, *p*-PPh), 6.73 (d, $^3J_{HH}$ = 8.7 Hz, 2H, C^2H^{tol}), 6.68 (d, $^3J_{HH}$ = 8.7 Hz, C^3H^{tol}), 5.63 (m, 2H, $C^{sp2}H^{cod}$), 2.81 (m, 2H, $C^{sp2}H^{cod}$), 2.05 (br, 4H, $CH_2^{cod,endo}$), 1.99 (s, 3H, CH_3^{tol}), 1.63 (m, 2H, $CH_2^{cod,exo}$), 1.43 (br, 2H, $CH_2^{cod,exo}$). ^{13}C NMR (C_6D_6, 298 K): δ_C 140.9 (d, $^2J_{CP}$ = 11.6 Hz,

Open Access Article. Published on 25 July 2022. Downloaded on 1/21/2026 6:06:26 AM.
This article is licensed under a Creative Commons Attribution-NonCommercial 3.0 Unported Licence.

$C^{1,\,tol}$), 134.1 (d, $^2J_{CP}$ = 12.0 Hz, $C^{2,\,PhP}$), 132.6 ($C^{4,\,tol}$), 131.5 (d, $^1J_{CP}$ = 50.8 Hz, $C^{1,\,PhP}$), 131.4 (d, $^3J_{CP}$ = 2.2 Hz, $C^{3,\,PhP}$), 130.2 ($C^{2,\,tol}$), 129.1 ($C^{4,\,PhP}$), 120.3 ($C^{3,\,tol}$), 94.5(d, $^3J_{CP}$ = 14.9 Hz, $C^{sp2,\,cod}$), 54.7 ($C^{sp2,\,cod}$), 34.1 (d, $^4J_{CP}$ = 3.3 Hz $C^{sp3,\,cod}$), 30.0 (d, $^4J_{CP}$ = 2.1 Hz $C^{sp3,\,cod}$), 21.0 (CH_3^{tol}). $^{31}P\{^1H\}$ NMR (C_6D_6, 298 K): δ_P 43.9 (s).

Synthesis of [IrCl(SiMe$_3$NP)(cod)] (2). A dichloromethane solution (15 mL) of [Ir(μ-Cl)(cod)]$_2$ (479 mg, 0.713 mmol, 671.70 g mol^{-1}) was added with $SiMe_3NP$ (546 mg, 1.50 mmol, 363.51 g mol^{-1}). The resulting orange solution was stirred for 3 h, evaporated up to 3 mL and added with hexane (10 mL), affording an orange solid which was filtered off, washed with hexane (12 mL), dried *in vacuo* and finally identified as [IrCl(SiMe$_3$NP)(cod)] (839 mg, 84% yield). Found: C 51.97, H 5.43, N 1.92. Calcd for: $C_{30}H_{38}ClIrNPSi$ (699.36 g mol^{-1}): C 51.52, H 5.48, N 2.00. ^1H NMR (C_6D_6 298 K): δ_H 7.68 (m, 4H, *o*-PPh), 6.94–6.87 (6H tot; 4H *m*-PPh, 2H *p*-PPh), 6.72 (dd, 2H, $^3J_{HH}$ = 8.2 Hz, $^4J_{HP}$ = 1.4 Hz, C^2H^{tol}), 6.45 (d, 2H, C^3H^{tol}, $^3J_{HH}$ = 8.2 Hz), 5.48 (m, 2H, $C^{sp2}H^{cod}$), 2.39 (m, 2H, $C^{sp2}H^{cod}$), 2.05–1.88 (4H tot; 2H, $C^{sp3}H^{cod\ endo}$; 2H, $C^{sp3}H^{cod\ exo}$) 1.81 (s, 3H, CH_3^{tol}), 1.51 (m, 2H, $C^{sp3}H^{cod\ exo}$), 1.22 (m, 2H, $C^{sp3}H^{cod\ endo}$), 0.70 (s, 9H, $SiCH_3$). $^{13}C\{^1H\}$ NMR (C_6D_6, 298 K): δ_C 141.1 (d, $^2J_{CP}$ = 9.4 Hz, $C^{1,\,tol}$), 136.0 (d, $^3J_{CP}$ = 11.6 Hz, $C^{2,\,PhP}$), 135.0 (d, $^1J_{CP}$ = 51.8 Hz, $C^{1,\,PhP}$), 133.7 (d, $^3J_{CP}$ = 2.5 Hz, $C^{2,\,tol}$), 130.6 (d, $^4J_{CP}$ = 1.9 Hz, $C^{4,\,PhP}$), 129.7 (d, $^4J_{CP}$ = 1.9 Hz, $C^{3,\,tol}$), 127.8 (d, $^3J_{CP}$ = 9.8 Hz, $C^{3,\,PhP}$), 93.8 (d, $^2J_{CP}$ = 15.73 Hz, $C^{sp2,\,cod}$), 53.6 ($C^{sp2,\,cod}$), 34.1 (d, $^3J_{CP}$ = 3.1 Hz, $C^{sp3,\,cod}$), 30.2 (d, $^3J_{CP}$ = 2.2 Hz, $C^{sp3,\,cod}$), 21.3 (CH_3^{tol}), 3.9 (d, $^2J_{CP}$ = 1.9 Hz, $SiCH_3$), $^{31}P\{^1H\}$ NMR (C_6D_6, 298 K): δ_P 62.2 (s).

Synthesis of [IrCl(HNP)$_2$(cod)] (3). A dichloromethane solution (5 mL) of [Ir(μ-Cl)(cod)]$_2$ (166 mg, 0.247 mmol, 671.70 g mol^{-1}) was added with HNP (304 mg, 1.04 mmol, 291.33 g mol^{-1}). The resulting yellow solution was stirred for 4 h, evaporated up to 2 mL and added with hexane (10 mL), affording a light yellow solid which was filtered off and washed with diethyl ether (15 mL), dried *in vacuo* and finally identified as [IrCl(HNP)$_2$(cod)] (301 mg, 66% yield). Found: C 59.99, H 5.42, N 3.15. Calcd for: $C_{46}H_{48}ClIrN_2P_2$ (918.50 g mol^{-1}): C 60.15, H 5.27, N 3.05. ^1H NMR (CD_2Cl_2, 298 K): δ_H 7.60–7.34 (10H tot; 8H, *o*-PPh; 2H, HNP), 7.33–7.01 (12H tot; 8H, *m*-PPh; 4H *p*-PPh), 6.75 (d, 4H, $^3J_{HH}$ = 8.2 Hz, C^3H^{tol}), 6.32 (d, 4H, $^3J_{HH}$ = 8.2 Hz, C^2H^{tol}), 3.43 (br, 4H, $C^{sp2}H^{cod}$), 2.32 (m, 4H, $C^{sp3}H^{cod\ endo}$), 2.15 (s, 3H, CH_3^{tol}), 1.88 (m 4H, $C^{sp3}H^{cod\ exo}$). $^{13}C\{^1H\}$ NMR (CD_2Cl_2, 298 K): δ_C 142.0 (br, $C^{1,\,tol}$), 132.7 (br, $C^{2,\,PhP}$), 130.3 (br, $C^{4,\,PhP}$), 130.0 ($C^{4,\,tol}$), 129.7 ($C^{3,\,tol}$), 128.4 ($C^{3,\,PhP}$), 118.7 ($C^{2,\,tol}$), 69.4 (br, $C^{sp2,\,cod}$), 33.2 ($C^{sp3,\,cod}$), 20.9 (CH_3^{tol}). $^{31}P\{^1H\}$ NMR (CD_2Cl_2, 298 K): δ_P 27.2 (br). ^1H NMR (CD_2Cl_2, 213 K): δ_H 7.77 (t, $^2J_{HP}$ = 6.6 Hz, 2H, HNP), 7.44 (m, 4H, *o*-PPh), 7.31–7.16 (12H tot; 4H, *o*-PPh; 4H *m*-PPh; 4H, *p*-PPh), 6.99 (t, 4H, $^3J_{HH}$ = 7.5 Hz, *m*-PPh), 6.75 (d, 4H, $^3J_{HH}$ = 8.1 Hz, C^3H^{tol}), 6.27 (d, 4H, $^3J_{HH}$ = 8.1 Hz, C^2H^{tol}), 3.37 (br, 4H, $C^{sp2}H^{cod}$), 2.36 (m, 4H, $C^{sp3}H^{cod\ endo}$), 2.12 (s, 3H, CH_3^{tol}), 1.91 (m 4H, $C^{sp3}H^{cod\ exo}$). $^{13}C\{^1H\}$ NMR (CD_2Cl_2, 213 K): δ_C 141.1 (t, $^2J_{CP}$ = 5.8 Hz, $C^{1,\,tol}$), 132.3 (t, $^2J_{CP}$ = 4.7 Hz, $C^{2,\,PhP}$),131.1 (d, $^1J_{CP}$ = 60.0 Hz, $C^{1,\,PhP}$), 130.9 (t, $^2J_{CP}$ = 4.8 Hz, $C^{2,\,PhP}$), 130.3 (d, $^1J_{CP}$ = 51.7 Hz, $C^{1,\,PhP}$), 130.1 ($C^{4,\,PhP}$), 129.7 ($C^{4,\,PhP}$), 129.3 ($C^{4,\,tol}$), 129.1 ($C^{3,\,tol}$), 128.0 (t, $^3J_{CP}$ = 5.2 Hz, $C^{3,\,PhP}$), 127.6 (t, $^3J_{CP}$ = 4.9 Hz, $C^{3,\,PhP}$), 117.8 ($C^{2,\,tol}$), 69.0 (t, $^2J_{CP}$ = 7.5 Hz, $C^{sp2,\,cod}$), 32.6 (br, $C^{sp3,\,cod}$), 20.5 (CH_3^{tol}); $^{31}P\{^1H\}$ NMR (CD_2Cl_2, 213 K): δ_P 27.9 (s).

Synthesis of [Ir(SiMe$_3$NP)$_2$(CO)$_3$][IrCl$_2$(CO)$_2$] (4[IrCl$_2$(CO)$_2$]). An orange dichloromethane solution (2 mL) of [IrCl(SiMe$_3$NP)(cod)] (174 mg, 0.249 mmol, 699.36 g mol^{-1}) was stirred under carbon monoxide (1 atm approx.) for 1 h. Hexane (15 mL) was added to the resulting pale yellow-green solution, affording a green oil that was washed with hexane (3 × 5 mL) eventually yielding a green solid, which was dried under vacuum and finally identified as [Ir(SiMe$_3$NP)$_2$(CO)$_3$][IrCl$_2$(CO)$_2$] (122 mg, 72% yield). Found: C 44.53, H 4.05, N 2.16. Calcd for: $C_{49}H_{52}Cl_2Ir_2N_2O_5P_2Si_2$ (1322.41 g mol^{-1}): C 44.50, H 3.96, N 2.12. ^1H NMR (CD_2Cl_2, 298 K): δ_H 7.65 (t, 4H, $^3J_{HH}$ = 7.5 Hz, *p*-PPh), 7.58 (8H t, $^3J_{HH}$ = 7.5 Hz, *m*-PPh), 7.45 (dd, 8H, $^3J_{HP}$ = 13.4 Hz, $^3J_{HH}$ = 7.5 Hz, *o*-PPh), 7.11 (d, 4H, $^3J_{HH}$ = 8.0 Hz, C^3H^{tol}), 6.93 (d, 4H, $^3J_{HH}$ = 8.0 Hz, C^2H^{tol}), 2.41 (s, 6H, CH_3^{tol}), −0.09 (s, 18H, $SiCH_3$). $^{13}C\{^1H\}$ NMR (CD_2Cl_2, 298 K): δ_C 173.5 (t, $^2J_{CP}$ = 11.1 Hz, P_2IrCO), 169.1 (Cl_2IrCO), 142.8 ($C^{1,\,tol}$), 138.3 ($C^{4,\,tol}$), 134.9 (t, $^1J_{CP}$ = 34.0 Hz, $C^{1,\,PhP}$), 133.7 ($C^{4,\,PhP}$), 133.3 (t, $^2J_{CP}$ = 6.4 Hz, $C^{2,\,PhP}$), 131.11 ($C^{3,\,tol}$), 131.08 (d, $^3J_{CP}$ = 3.0 Hz $C^{2,\,tol}$), 130.0 (t, $^3J_{CP}$ = 5.6 Hz, $C^{3,\,PhP}$), 21.7 (CH_3^{tol}), 3.4 (d, $^3J_{CP}$ = 0.5 Hz, $SiCH_3$). $^{31}P\{^1H\}$ NMR (CD_2Cl_2, 298 K): δ_P 42.9 (s).

Synthesis of [IrH{κ^2*C*,*P*-HN(4-C$_6$H$_3$CH$_3$)PPh$_2$}(cod)(CH$_3$CN)][PF$_6$] (5PF$_6$). *Method (1)*: A dichloromethane solution (5 mL) of [Ir(CH$_3$CN)$_2$(cod)][PF$_6$] (251 mg, 0.476 mmol, 527.47 g mol^{-1}) at 223 K was added with a dichloromethane solution (5 mL) of HNP (139 mg, 0.476 mmol, 291.33 g mol^{-1}) at 223 K. The resulting dark red solution was stirred for 2 h at 233 K. Afterwards, the solution was allowed to warm up to room temperature and was finally stirred for 30 min. The resulting orange solution was dried *in vacuo* and the residue was washed with diethyl ether (3 × 5 mL), dried *in vacuo* and finally identified as [IrH{κ^2*C*,*P*-HN(4-C$_6$H$_3$CH$_3$)PPh$_2$}(cod)(CH$_3$CN)][PF$_6$] (348 mg, 94% yield).

Method (2): An acetonitrile solution (8 mL) of [IrCl(HNP)(cod)] (227 mg, 0.361 mmol, 627.18 g mol^{-1}) was added with $TlPF_6$ (126 mg, 0.361 mmol, 349.94 g mol^{-1}). The resulting pale yellow suspension was stirred for 1 h and evaporated *in vacuo*, affording a colorless solid that was extracted with dichloromethane (3 × 3 mL). The resulting pale yellow liquid phase was evaporated up to 1 mL and added with diethyl ether (5 mL), affording a colourless solid which was filtered off, washed with diethyl ether (3 × 5 mL), dried *in vacuo* and finally identified as [IrH{κ^2*C*,*P*-HN(4-C$_6$H$_3$CH$_3$)PPh$_2$}(cod)(CH$_3$CN)][PF$_6$] (252 mg, 89% yield). Found: C 44.95, H 4.21, N 3.69. Calcd for $C_{29}H_{33}F_6IrN_2P_2$ (777.74 g mol^{-1}): C 44.78, H 4.28, N 3.60. ^1H NMR (CD_2Cl_2, 298 K): δ_H 7.79 (dd, 2H, $^3J_{HP}$ = 12.9 Hz, $^3J_{HH}$ = 7.3 Hz, 2H *o*-PPh), 7.71–7.66 (3H tot; 2H, *m*-PPh; 1H, *p*-PPh), 7.65–7.55 (5H tot; 2H, *o*-PPh; 2H, *m*-PPh; 1H, *p*-PPh), 6.88 (d, 1H, $^3J_{HH}$ = 7.8 Hz, C^6H^{tol}), 6.83 (d, 1H, $^3J_{HH}$ = 7.8 Hz, C^5H^{tol}), 6.70 (br, 1H, C^3H^{tol}), 5.77 (m, 1H, $C^{sp2}H^{cod,\ up\text{-}trans}$), 5.40 (m, 1H, $C^{sp2}H^{cod\ down\text{-}trans}$), 5.22 (br, 1H, NH), 4.76 (dd, $^3J_{HP}$ = 9.5 Hz, $^3J_{HH}$ = 7.4 Hz 1H, $C^{sp2}H^{cod\ up\text{-}cis}$), 4.61 (m, 1H, $C^{sp2}H^{cod\ down\text{-}cis}$), 2.68 (m, 6H, $C^{sp3}H^{cod}$), 2.49 (m,

This journal is © The Royal Society of Chemistry 2022

Open Access Article. Published on 25 July 2022. Downloaded on 1/21/2026 6:06:26 AM.
This article is licensed under a Creative Commons Attribution-NonCommercial 3.0 Unported Licence.

2H, $C^{sp3}H^{cod}$), 2.23 (s, 3H, CH_3^{tol}), 1.92 (s, 3H, CH_3CN), −16.07 (d, 1H, $^2J_{HP}$ = 10.6 Hz, IrH). $^{13}C\{^1H\}$ NMR (CD_2Cl_2, 298 K): δ_C 151.6 (d, $^2J_{CP}$ = 16.2 Hz, $C^{1,\ tol}$), 135.2 ($C^{3,\ tol}$), 133.6 (d, $^4J_{CP}$ = 2.8 Hz, $C^{4,\ PhP}$), 133.2 (d, $^2J_{CP}$ = 12.5 Hz, $C^{2,\ PhP}$), 132.8 (d, $^4J_{CP}$ = 2.9 Hz, $C^{4,\ PhP}$), 131.21 (d, $^2J_{CP}$ = 11.2 Hz, $C^{2,\ PhP}$), 131.19 (d, $^1J_{CP}$ = 60.4 Hz, $C^{1,\ PhP}$), 130.4 (d, $^1J_{CP}$ = 60.2 Hz, $C^{1,\ PhP}$), 130.2 (d, $^3J_{CP}$ = 11.8 Hz, $C^{3,\ PhP}$), 130.13 (d, $^2J_{CP}$ = 11.2 Hz, $C^{3,\ PhP}$), 130.09 ($C^{4,\ tol}$), 127.4 (br, $C^{5,\ tol}$), 122.2 ($CH_3\underline{C}N$), 122.0 (d, $^2J_{CP}$ = 2.9 Hz, $C^{2,\ tol}$) 111.5 (d, $^3J_{CP}$ = 14.5 Hz, $C^{6,\ tol}$), 100.6 (d, $^2J_{CP}$ = 10.6 Hz, $C^{sp2,\ cod\ up\text{-}trans}$), 98.8 (d, $^2J_{CP}$ = 12.7 Hz, $C^{sp2,\ cod\ down\text{-}trans}$), 92.93 (br, $C^{sp2,\ cod\ up\ cis}$), 92.87 ($C^{sp2,\ cod\ down\text{-}cis}$), 33.3 (d, $^3J_{CP}$ = 2.2 Hz, $C^{sp3,\ cod}$), 32.4 (br, $C^{sp3,\ cod}$), 30.3 (d, $^3J_{CP}$ = 2.8 Hz, $C^{sp3,\ cod}$), 28.8 (d, $^3J_{CP}$ = 1.3 Hz, $C^{sp3,\ cod}$), 21.2 (CH_3^{tol}), 2.31 (d, $^3J_{CP}$ = 1.2 Hz, $SiCH_3$), 3.6 ($\underline{C}H_3CN$). $^{31}P\{^1H\}$ NMR (CD_2Cl_2, 298 K): δ_P 62.5 (s, NP), −144.7 (hept, $^1J_{PF}$ = 710.1 Hz, PF_6^-).

Synthesis of [IrH{κ²*C*,*P*-SiMe₃N(4-C₆H₃CH₃)PPh₂}(cod)(CH₃CN)][PF₆] (6PF₆). *Method (1)*: A dichloromethane solution (10 mL) of $[Ir(CH_3CN)_2(cod)][PF_6]$ (206 mg, 0.390 mmol, 527.47 g mol^{-1}) was added with $SiMe_3NP$ (142 mg, 0.391 mmol, 363.51 g mol^{-1}). The resulting dark red solution was stirred for 1 h, evaporated up to 3 mL and added with hexane (5 mL), affording a pale red solid which was filtered off, washed with hexane (3 × 5 mL), dried *in vacuo* and finally identified as $[IrH\{\kappa^2C,P\text{-}SiMe_3N(4\text{-}C_6H_3CH_3)PPh_2\}(cod)(CH_3CN)][PF_6]$ (289 mg, 87% yield).

Method (2): An acetonitrile solution (5 mL) of $[IrCl\{SiMe_3N(4\text{-}C_6H_4CH_3)PPh_2\}(cod)]$ (157 mg, 0.224 mmol, 699.18 g mol^{-1}) was added with $TlPF_6$ (78.5 mg, 0.224 mmol, 349.94 g mol^{-1}). The resulting red solution was stirred for 1 h and evaporated *in vacuo*, affording a pale red solid which was eventually extracted with dichloromethane (2 × 5 mL). The resulting red liquid phase was evaporated up to 2 mL and added with hexane (5 mL), affording a pale red solid which was filtered off, washed with hexane (3 × 5 mL), dried *in vacuo* and finally identified as $[IrH\{\kappa^2C,P\text{-}SiMe_3N(4\text{-}C_6H_3CH_3)PPh_2\}(cod)(CH_3CN)][PF_6]$ (154 mg, 81% yield). Found: C 44.99, H 4.95, N 3.22. Calcd for: $C_{32}H_{41}F_6IrN_4P_2Si$ (849.92 g mol^{-1}): C 45.22, H 4.86, N 3.30. ^1H NMR (CD_2Cl_2, 298 K): δ_H 7.89 (m, 2H, *o*-PPh), 7.73 (td, 2H, $^3J_{HH}$ = 7.3 Hz, $^4J_{HP}$ = 2.9 Hz *m*-PPh), 7.69–7.49 (6H tot; 2H, *o*-PPh; 2H, *m*-PPh; 2H, *p*-PPh), 7.14 (d, 1H, $^3J_{HH}$ = 8.2 Hz, C^6H^{tol}), 6.91 (d, 1H, $^3J_{HH}$ = 8.2 Hz, C^5H^{tol}), 6.72 (br, 1H, C^3H^{tol}), 5.54 (m, 1H, $C^{sp2}H^{cod\ up\text{-}trans}$), 5.37 (m, 1H, $C^{sp2}H^{cod\ down\text{-}trans}$), 4.69 (m, 1H, $C^{sp2}H^{cod\ down\text{-}cis}$), 4.09 (t, 1H, $^3J_{HH}$ = 7.8 Hz, $C^{sp2}H^{cod\ up\text{-}cis}$), 2.76 (m, 2H, $C^{sp3}H^{cod}$), 2.50 (m, 4H, $C^{sp3}H^{cod}$), 2.25 (s, 3H, CH_3^{tol}), 2.12 (m, 2H, $C^{sp3}H^{cod}$), 1.80 (s, 3H, CH_3CN), 0.14 (s, 9H, $SiCH_3$), −16.43 (d, 1H, $^2J_{HP}$ = 11.2 Hz, IrH). $^{13}C\{^1H\}$ NMR (CD_2Cl_2, 298 K): δ_C 154.8 (d, $^2J_{CP}$ = 16.2 Hz, $C^{1,\ tol}$), 135.7 ($C^{3,\ tol}$), 132.8 (d, $^1J_{CP}$ = 73.7 Hz, $C^{1,\ PhP}$), 132.6 (d, $^4J_{CP}$ = 2.8 Hz, $C^{4,\ PhP}$), 132.1 (d, $^4J_{CP}$ = 2.9 Hz, $C^{4,\ PhP}$), 131.8 (d, $^2J_{CP}$ = 11.8 Hz, $C^{2,\ PhP}$), 131.2 (d, $^1J_{CP}$ = 74.7 Hz, $C^{1,\ PhP}$),131.1 (d, $^3J_{CP}$ = 10.5 Hz, $C^{2,\ PhP}$), 130.5 ($C^{4,\ tol}$), 129.8 (d, $^3J_{CP}$ = 11.0 Hz, $C^{3,\ PhP}$), 129.3 (d, $^2J_{CP}$ = 11.9 Hz, $C^{3,\ PhP}$), 127.1 (d, $^2J_{CP}$ = 3.5 Hz, $C^{2,\ tol}$), 126.2 ($C^{5,\ tol}$), 121.4 ($CH_3\underline{C}N$), 114.4 (d, $^3J_{CP}$ = 16.1 Hz, $C^{6,\ tol}$), 101.1 (d, $^2J_{CP}$ = 10.6 Hz, $C^{sp2,\ cod\ down\text{-}trans}$), 100.6 (d, $^2J_{CP}$ = 12.2 Hz, $C^{sp2,\ cod\ up\text{-}trans}$), 94.9 (d, $^2J_{CP}$ = 12.2 Hz, $C^{sp2,\ cod\ up\text{-}trans}$), 94.4 ($C^{sp2,\ cod\ down\text{-}cis}$), 32.7 (d, $^3J_{CP}$ = 2.5 Hz, $C^{sp3,\ cod}$), 31.5 (d, $^3J_{CP}$ = 1.2 Hz, $C^{sp3,\ cod}$), 29.7 (d, $^3J_{CP}$ = 2.7 Hz, $C^{sp3,\ cod}$), 28.1 (d, $^3J_{CP}$ = 2.0 Hz, $C^{sp3,\ cod}$), 20.7 (CH_3^{tol}), 2.64 (d, $^3J_{CP}$ = 1.2 Hz, $SiCH_3$), 2.63 ($\underline{C}H_3CN$). $^{31}P\{^1H\}$ NMR (CD_2Cl_2, 298 K): δ_P 73.9 (s, NP), −144.7 (hept, $^1J_{PF}$ = 710.1 Hz, PF_6^-).

Formation of [Ir(HNP)₃(cod)]⁺ (9⁺). In a 5 mm NMR tube, a CD_2Cl_2 solution (0.4 mL) of $[Ir(CH_3CN)_2(cod)][PF_6]$ (23.7 mg, 0.0450 mol, 527.47 g mol^{-1}) at 223 K was added to a CD_2Cl_2 solution (0.4 mL) of HNP (39.3 mg, 0.135 mmol, 291.33 g mol^{-1}) at 223 K. Soon after the addition, the NMR tube was introduced into the NMR spectrometer at 233 K, observing the formation of $[Ir(HNP)_3(cod)]^+$ (**9⁺**, 80 mol%) along with unidentified by-products (total 15 mol%). ^1H NMR (CD_2Cl_2, 223 K): δ_H 7.63 (br, 6H, *o*-PPh), 7.45 (t, 6H, $^3J_{HH}$ = 6.9 Hz, *p*-PPh), 7.31 (t, 12H, $^3J_{HH}$ = 7.5 Hz, *m*-PPh), 7.15–7.00 (7H tot; 6H. *o*-PPh; 1H, HNP), 6.82 (d, 6H, $^3J_{HH}$ = 8.0 Hz, C^3H^{tol}), 6.20 (d, 6H, $^3J_{HH}$ = 8.0 Hz, C^2H^{tol}), 3.41 (br, 4H, $C^{sp2}H^{cod}$), 2.73 (br, 2H, $C^{sp3}H^{cod}$), 2.45 (m, 4H, $C^{sp3}H^{cod}$), 2.19 (s, 9H, CH_3^{tol}), 1.55 (m, 2H, $C^{sp3}H^{cod}$). $^{13}C\{^1H\}$ NMR (CD_2Cl_2, 223 K): δ_C 139.1 (d, $^2J_{CP}$ = 10.6 Hz, $C^{1,\ tol}$), 131.54 ($C^{4,\ tol}$), 131.47 ($C^{4,\ PhP}$), 131.42 ($C^{2,\ PhP}$), 129.8 ($C^{3,\ tol}$), 129.0 ($C^{3,\ PhP}$), 128.6 ($C^{2,\ PhP}$), 118.6 ($C^{2,\ tol}$), 74.2 ($C^{sp2,\ cod}$), 38.1 ($C^{sp3,\ cod}$), 28.7 ($C^{sp3,\ cod}$), 20.5 (CH_3^{tol}). $^{31}P\{^1H\}$ NMR (CD_2Cl_2, 223 K): δ_P 18.5 (br, 3P, HNP).

Formation of [IrH{κ²*C*,*P*-SiMe₃N(4-C₆H₃CH₃)PPh₂}(cod)(HNP)]⁺ (10⁺). A CD_2Cl_2 solution (0.5 mL) of $[IrH\{\kappa^2C,P\text{-}HN(4\text{-}C_6H_3CH_3)PPh_2\}(cod)(CH_3CN)][PF_6]$ (28.2 mg, 0.0363 mmol, 777.74 g mol^{-1}) at 223 K was added with a CD_2Cl_2 solution (0.5 mL) of $SiMe_3NP$ (13.2 mg, 0.0363 mmol, 363.51 g mol^{-1}) at 223 K. Soon after, the NMR tube was introduced into a NMR spectrometer at 223 K. The formation of $[IrH\{\kappa^2C,P\text{-}SiMe_3N(4\text{-}C_6H_3CH_3)PPh_2\}(cod)(HNP)]$ (**10⁺**) was observed over the following 5 h. ^1H NMR (CD_2Cl_2, 223 K): δ_H 8.10 (br, 2H, *o*-P^1Ph), 7.81–7.24 (17H tot; 4H, *o*-P^2Ph; 4H, *m*-P^2Ph, 2H, *p*-P^2Ph, 4H, *m*-P^1Ph, 2H, *p*-P^1Ph; 1H, (d, δ 7.42), $^3J_{HH}$ = 8.3 Hz, $C^6H^{tol\text{-}P1}$), 7.19 (br, 1H, *o*-P^1Ph), 7.07 (d, 1H, $^3J_{HH}$ = 8.3 Hz, $C^5H^{tol\text{-}P1}$), 6.60 (d, 2H, $^3J_{HH}$ = 8.1 Hz, $C^3H^{tol\text{-}P2}$), 6.55 (br, 1H, *o*-P^1Ph), 6.35 (br, 1H, $C^3H^{tol\text{-}P1}$), 5.77 (d, 2H, $^3J_{HH}$ = 8.1 Hz, $C^2H^{tol\text{-}P2}$), 5.22(br, 1H, $C^{sp2}H^{cod\ up}$), 4.81 (d, 1H, $^2J_{HP}$ = 17.0, HNP), 4.13 (3H tot; 1H, $C^{sp2}H^{cod\ up}$; 2H, $C^{sp2}H^{cod\ down}$), 2.87 (m, 2H, $C^{sp3}H^{cod}$), 2.52 (m, 3H, $C^{sp3}H^{cod}$), 2.29 (s, 3H, $CH_3^{tol\text{-}P1}$), 2.03 (s, 3H, $CH_3^{tol\text{-}P2}$), 1.87 (m, 3H, $C^{sp3}H^{cod}$), 0.25 (br, 9H, $SiCH_3$), −10.18 (dd, 1H, $^2J_{HPtrans}$ = 105.5 Hz, $^2J_{HPcis}$ = 12.4 Hz, IrH). $^{13}C\{^1H\}$ NMR (CD_2Cl_2, 223 K): δ_C 154.4 (d, $^2J_{CP}$ = 16.0 Hz, $C^{1,\ tol\text{-}P1}$), 138.9 (d, $^2J_{CP}$ = 10.6, $C^{1,\ tol\text{-}P2}$), 138.45 (d, $^1J_{CP}$ = 70.8 Hz, $C^{1,\ PhP1}$), 138.41 (d, $^1J_{CP}$ = 72.1 Hz, $C^{1,\ PhP1}$), 136.0 ($C^{3I,\ tol\text{-}P1}$), 132.3 ($C^{3,\ PhP1}$), 132.1 ($C^{3,\ PhP1}$), 130.7 ($C^{2,\ PhP1}$), 130.4 ($C^{3,\ PhP2}$), 130.24 ($C^{2,\ PhP1}$), 130.17 ($C^{4,\ tol\text{-}P1}$), 129.6 ($C^{2,\ PhP1}$), 129.2 ($C^{3,\ tol\text{-}P2}$), 128.7 ($C^{4,\ tol\text{-}P2}$), 128.0 ($C^{2,\ PhP2}$), 127.0 ($C^{3,\ tol\text{-}P1}$), 124.4 (dd, $^2J_{CP}$ = 13.4 Hz, $^2J_{CP}$ = 10.3 Hz, $C^{2I,\ tol\text{-}P1}$), 117.9 (d, $^2J_{CP}$ = 5.0 Hz, $C^{2,\ tol\text{-}P2}$), 116.5 (d, $^2J_{CP}$ = 16.0 Hz, $C^{2,\ tol\text{-}P1}$), 96.2 (d, $^2J_{CP}$ = 8.6 Hz, $C^{sp2,\ cod\ up}$), 93.0 ($C^{sp2,\ cod\ down}$), 91.9 ($C^{sp2,\ cod\ down}$), 89.5 ($C^{sp2,\ cod\ up}$), 37.4 ($C^{sp3,\ cod}$), 31.6 (d, $^3J_{CP}$ = 34.3 Hz, $C^{sp3,\ cod}$), 28.4 ($C^{sp3,\ cod}$), 20.6 ($CH_3^{tol\text{-}P1}$), 20.4 ($CH_3^{tol\text{-}P2}$), 2.6 ($SiCH_3$). $^{31}P\{^1H\}$ NMR (CD_2Cl_2, 223 K): δ_P 66.6 (d, 1P, $^2J_{PP}$ = 22.2 Hz, $SiNP^1$), 1.2 (d, 1P, $^2J_{PP}$ = 22.2 Hz, HNP^2).

Open Access Article. Published on 25 July 2022. Downloaded on 1/21/2026 6:06:26 AM.
This article is licensed under a Creative Commons Attribution-NonCommercial 3.0 Unported Licence.

Synthesis of $[Ir(SiMe_3NP)_2(CH_3CN)_2][PF_6]$ (11PF_6). A dichloromethane suspension (5 mL) of $[Ir(CH_3CN)_2(coe)_2][PF_6]$ (136 mg, 0.212 mmol, 639.68 g mol^{-1}) was added with $SiMe_3NP$ (154 mg, 0.424 mmol, 363.51 g mol^{-1}). The resulting orange solution was stirred for 30 min, evaporated up to approx. 2 mL and added with hexane (5 mL), affording an orange solid which was filtered off, washed with diethyl ether (3 × 5 mL), dried *in vacuo* and finally identified as $[Ir(SiMe_3NP)_2(CH_3CN)_2][PF_6]$ (149 mg, 61% yield). Found: C 49.95, H 5.19, N 4.78. Calcd for $C_{48}H_{58}F_6IrN_4P_3Si_2$ (1146.30 g mol^{-1}): C 50.29, H 5.10, N 4.89. ^1H NMR (CD_2Cl_2, 298 K): δ_H 7.55 (m, 8H, *o*-PPh), 7.47–7.40 (12H tot; 8H, *m*-PPh; 4H, *p*-PPh), 7.01 (d, 4H, $^3J_{HH}$ = 8.4 Hz, C^2H^{tol}), 6.97 (d, 4H, $^3J_{HH}$ = 8.4 Hz, C^3H^{tol}), 2.30 (s, 6H, CH_3^{tol}), 1.42 (s, 6H, CH_3CN), 0.03 (s, 18H, $Si(CH_3)_3$). $^{13}C\{^1H\}$ NMR (CD_2Cl_2, 298 K): δ_C 142.7 ($C^{1,\ tol}$), 136.6 ($C^{4,\ tol}$), 135.0 (t, $^1J_{CP}$ = 26.5 Hz, $C^{1,\ PhP}$), 133.2 (t, $^2J_{CP}$ = 6.5 Hz, $C^{2,\ PhP}$), 132.9 ($C^{3,\ tol}$), 130.8 ($C^{4,\ PhP}$), 129.8 ($C^{2,\ tol}$), 128.6 (t, $^3J_{CP}$ = 4.8 Hz, $C^{3,\ PhP}$), 115.7 ($CH_3\underline{C}N$), 21.5 (CH_3^{tol}), 4.2 ($\underline{C}H_3CN$), 2.7 ($SiCH_3$). $^{31}P\{^1H\}$ NMR (CD_2Cl_2, 298 K): δ_P 61.8 (s, 2P, NP), −144.7 (hept, $^1J_{PF}$ = 710.1 Hz, PF_6^-).

Synthesis of *OC*-6-34-$[IrH\{\kappa^3C,P\text{-}HN(4\text{-}C_6H_3CH_3)PPh_2\}(CH_3CN)(HNP)_2][PF_6]$ (12PF_6). An acetonitrile solution (5 mL) of $[Ir(CH_3CN)_2(coe)_2][PF_6]$ (108 mg, 0.169 mmol, 639.68 g mol^{-1}) was added with HNP (148 mg, 0.508 mmol, 291.33 g mol^{-1}) yielding a yellow solution which was stirred for 2 h, evaporated up to 2 mL and added with diethyl ether (5 mL). The resulting suspension was filtered and the yellow solid was washed with diethyl ether (3 × 5 mL), dried *in vacuo* and finally identified as *OC*-6-34-$[IrH\{\kappa^2C,P\text{-}HN(4\text{-}C_6H_3CH_3)PPh_2\}(CH_3CN)(HNP)_2][PF_6]$ (125 mg, 59% yield). Found: C 57.01, H 4.88, N 4.35. Calcd for $C_{59}H_{57}F_6IrN_4P_4$ (1252.21 g mol^{-1}): C 56.59, H 4.59, N 4.47. ^1H NMR (CD_3CN, 298 K): δ_H 7.90 (m, 2H, *o*-P^1Ph), 7.79 (td, 2H, $^3J_{HH}$ = 8.0 Hz, $^4J_{HP}$ = 2.2 Hz, *m*-P^1Ph), 7.71–7.57 (4H tot; 2H, *o*-P^3Ph; 2H, *m*-P^1Ph;), 7.57–7.49 (4H tot; 2H, *m*-P^3Ph, 2H, *p*-P^1Ph), 7.49–7.30 (4H tot; 2H, *o*-P^3Ph, 2H, *m*-P^2Ph), 7.32–7.11 (8H tot; 2H, *o*-P^1Ph; 2H, *m*-P^3Ph; 2H, *m*-P^2Ph; 2H, *p*-P^2Ph), 7.11–6.93 (4H tot; 2H, *o*-P^2Ph; 2H, *p*-P^3Ph), 6.88 (dd, 1H, $^3J_{HH}$ = 7.8 Hz, $^4J_{HP}$ = 2.3 Hz, $C^6H^{tol\text{-}P1}$), 6.83–6.72 (3H tot; 2H, *o*-P2Ph; 1H, $C^5H^{tol\text{-}P1}$), 6.69 (d, 2H, $^3J_{HH}$ = 8.2 Hz, $C^3H^{tol\text{-}P2}$), 6.66 (d, 2H, $^3J_{HH}$ = 8.2 Hz, $C^3H^{tol\text{-}P3}$), 6.38 (d, 1H, $^4J_{HP}$ = 5.2 Hz, $C^3H^{tol\text{-}P1}$), 6.28 (br, 1H, HNP^1), 5.89 (d, 2H, $^3J_{HH}$ = 8.2 Hz, $C^2H^{tol\text{-}P2}$), 5.67 (d, 2H, $^3J_{HH}$ = 8.2 Hz, $C^2H^{tol\text{-}P3}$), 5.17 (d, 1H, $^2J_{HP}$ = 19.6 Hz, HNP^2), 4.64 (d, 1H, $^2J_{HP}$ = 18.5 Hz, HNP^3), 2.11 (s, 3H, $CH_3^{tol\text{-}P3}$), 2.10 (s, 3H, $CH_3^{tol\text{-}P1}$), 2.07 (s, 3H, $CH_3^{tol\text{-}P2}$), 1.64 (s, 3H, CH_3CN), −11.83 (dt, 1H, $^2J_{HP}$ = 150.5 Hz, $^2J_{HP}$ = 16.2 Hz). $^{13}C\{^1H\}$ NMR (CD_3CN, 298 K): δ 149.8 (dd, $^2J_{CP}$ = 14.3 Hz, $^4J_{CP}$ = 2.1 Hz, $C^{1,\ tol\text{-}P1}$), 140.5 (d, $^2J_{CP}$ = 11.0 Hz, $C^{1,\ tol\text{-}P3}$), 140.2 (d, $^2J_{CP}$ = 11.1 Hz, $C^{1,\ tol\text{-}P2}$), 137.9 (dd, $^3J_{CP}$ = 2.6 Hz, $^5J_{CP}$ = 0.9 Hz, $C^{3,\ tol\text{-}P1}$), 133.7 (d, $^3J_{CP}$ = 2.7 Hz $C^{3,\ PhP1}$), 133.6 (d, $^2J_{CP}$ = 9.9 Hz, $C^{2,\ PhP2}$), 133.4 (dd, $^2J_{CP}$ = 11.2 Hz, $^4J_{CP}$ = 0.9 Hz, $C^{2,\ PhP3}$), 133.3 (d, $^2J_{CP}$ = 10.7 Hz, $C^{2,\ PhP1}$), 132.6 (d, $^4J_{CP}$ = 2.6 Hz $C^{4,\ PhP2}$), 132.53–131.27 ($C^{2,\ PhP1}$, $C^{2,\ PhP3}$, $C^{2,\ PhP2}$, $C^{4,\ PhP1}$, $C^{4,\ PhP3}$), 132.1 (d, $^2J_{CP}$ = 2.0 Hz, $C^{2,\ PhP3}$), 131.7 ($C^{4,\ tol\text{-}P3}$), 131.5 (d, $^4J_{CP}$ = 2.3 Hz, $C^{4,\ PhP3}$), 131.3 ($C^{4,\ tol\text{-}P2}$), 131.0 (d, $^3J_{CP}$ = 9.3 Hz, $C^{3,\ PhP2}$), 130.8 (d, $^3J_{CP}$ = 11.3 Hz, $C^{3,\ PhP1}$), 130.47 ($C^{4,\ PhP2}$), 130.44 ($C^{3,\ tol\text{-}P2}$), 130.34 ($C^{4,\ PhP1}$), 130.2($C^{3,\ tol\text{-}P3}$), 129.80 (d $^3J_{CP}$ = 11.5 Hz, $C^{3,\ PhP3}$), 129.75 ($C^{4,\ tol\text{-}P1}$), 129.6 (d, $^3J_{CP}$ = 10.6 Hz, $C^{3,\ PhP2}$), 128.6 (d, $^5J_{CP}$ = 9.8 Hz, $C^{4,\ PhP3}$), 127.0 (d, $^4J_{CP}$ = 1.5 Hz, $C^{3,\ tol\text{-}P1}$), 126.0 (d, $^3J_{CP}$ = 4.9 Hz, $C^{2,\ tol\text{-}P1}$), 121.1 ($CH_3\underline{C}N$), 119.6 (d, $^3J_{CP}$ = 5.3 Hz, $C^{2,\ tol\text{-}P3}$), 119.0 (d, $^3J_{CP}$ = 5.4 Hz, $C^{2,\ tol\text{-}P2}$), 112.2 (d, $^3J_{CP}$ = 14.0 Hz, $C^{6,\ tol\text{-}P1}$), 21.4 ($CH_3^{tol\text{-}P1}$), 20.8 ($CH_3^{tol\text{-}P3}$, $CH_3^{tol\text{-}P2}$), 3.8 ($\underline{C}H_3CN$). $^{31}P\{^1H\}$ NMR (CD_3CN, 298 K): δ_P 49.8 (t, 1P, $^2J_{CP}$ = 11.5 Hz, NP^1), 19.8 (dd, 1P, $^2J_{CP}$ = 16.0 Hz, $^2J_{CP}$ = 11.5 Hz, NP^2), 11.2 (dd, 1P, $^2J_{CP}$ = 16.0 Hz, $^2J_{CP}$ = 11.5 Hz, NP_3), −144.7 (hept, $^1J_{PF}$ = 710.1 Hz, PF_6^-).

Synthesis of *OC*-6-52-$[IrH\{\kappa^2C,P\text{-}NH(4\text{-}C_6H_3CH_3)PPh_2\}(CH_3CN)(HNP)_2][PF_6]$ (13PF_6). *Method (1)*: A dichloromethane suspension (5 mL) of $[Ir(CH_3CN)_2(coe)_2][PF_6]$ (116 mg, 0.181 mmol, 639.68 g mol^{-1}) was added with HNP (158 mg, 0.542 mmol, 291.33 g mol^{-1}) giving a yellow solution, which was stirred for 36 h, evaporated up to 2 mL and added with hexane (10 mL). The resulting suspension was filtered and the yellow solid washed with diethyl ether (5 mL) and hexane (5 mL), dried *in vacuo* and finally identified as *OC*-6-52-$[IrH\{\kappa^2C,P\text{-}HN(4\text{-}C_6H_3CH_3)PPh_2\}(CH_3CN)(HNP)_2][PF_6]$ (132 mg, 58% yield). Found: C 57.01, H 4.75, N 4.92. Calcd for $C_{59}H_{57}F_6IrN_4P_4$ (1252.21 g mol^{-1}): C 56.59, H 4.59, N 4.47. ^1H NMR (CD_2Cl_2, 298 K): δ_H 7.47–7.21 (22H tot; 4H, *o*-P^1Ph; 4H, *o*-$P^{2/3}$Ph; 4H, *m*-P^1Ph; 4H, *m*-$P^{2/3}$Ph; 2H, *p*-P^1Ph; 4H, *p*-$P^{2/3}$Ph), 7.14 (tt, 4H, $^3J_{HH}$ = 7.6 Hz, $^4J_{HP}$ = 1.7 Hz, *m*-$P^{2/3}$Ph), 6.99–6.86 (5H tot; 4H, *o*-$P^{2/3}$Ph 1H, $C^6H^{tol\text{-}P1}$), 6.78 (d, 1H, $^3J_{HH}$ = 8.0 Hz, $C^5H^{tol\text{-}P1}$), 6.66 (d, $^3J_{HH}$ = 8.0 Hz, 4H, $C^3H^{tol\text{-}P2/3}$), 6.23 (s, 1H, $C^3H^{tol\text{-}P1}$), 5.95 (d, $^3J_{HH}$ = 8.0 Hz, 4H, $C^2H^{tol\text{-}P2/3}$), 5.57 (d, 1H, $^2J_{HP}$ = 2.2 Hz, HNP^1), 5.18 (t, $^2J_{HP}$ = 8.3 Hz, 2H $HNP^{2/3}$), 2.08 (s, 6H $CH_3^{tol\text{-}P2/3}$), 1.95 (s, 3H, $CH_3^{tol\text{-}P1}$), 1.56 (s, 3H, CH_3CN), −9.86 (dt, 1H, $^2J_{HP}$ = 133.0 Hz, $^2J_{HP}$ = 18.6 Hz). $^{13}C\{^1H\}$ NMR (CD_2Cl_2, 298 K): δ_H 151.8 ($C^{1,\ tol\text{-}P1}$), 145.0 ($C^{3,\ tol\text{-}P1}$), 139.8 (t, $^3J_{CP}$ = 3.1 Hz, $C^{1,\ tol\text{-}P2/3}$), 139.1 ($C^{1,\ PhP}$), 132.5 (dd, $^2J_{CP}$ = 11.4 Hz, $^4J_{CP}$ = 5.7 Hz, $C^{2,\ PhP2/3}$), 131.1 (dd, $^2J_{CP}$ = 6.4 Hz, $^4J_{CP}$ = 3.5 Hz $C^{2,\ PhP1}$), 130.9 ($C^{4,\ tol\text{-}P2/3}$), 131.2 ($C^{4,\ PhP1}$), 129.9 ($C^{5,\ tol\text{-}P1}$), 129.8 ($C^{4,\ PhP2/3}$), 129.6 ($C^{2,\ tol\text{-}P2/3}$), 129.0 (dd, $^4J_{CP}$ = 5.9 Hz, $^6J_{CP}$ = 4.8 Hz, $C^{3,\ PhP2/3}$), 128.5 (dd, $^4J_{CP}$ = 5.8 Hz, $^6J_{CP}$ = 4.6 Hz, $C^{3,\ PhP1}$), 126.1 ($C^{4,\ tol\text{-}P1}$), 120.8 ($CH_3\underline{C}N$), 118.8 ($C^{3,\ tol\text{-}P2/3}$), 113.5 (dd, $^2J_{CP}$ = 10.0 Hz, $^2J_{CP}$ = 1.6 Hz, $C^{2,\ tol\text{-}P1}$), 111.7 (d, $^3J_{CP}$ = 13.4 Hz, $C^{6,\ tol\text{-}P1}$), 21.3 ($CH_3^{tol\text{-}P1}$), 20.8 ($CH_3^{tol\text{-}P2/3}$), 2.5 ($\underline{C}H_3CN$). $^{31}P\{^1H\}$ NMR (CD_2Cl_2, 298 K): δ_P 43.4 (t, 1P, $^2J_{PP}$ = 16.0 Hz, NP^1), 19.7 (d, 2P, $^2J_{PP}$ = 16.0 Hz, $NP^{2/3}$), −144.7 (hept, $^1J_{PF}$ = 710.1 Hz, PF_6^-).

Method (2): A CD_2Cl_2 solution (0.4 mL) of 12PF_6 (14.8 mg, 0.0118 mmol, 1252.21 g mol^{-1}) was allowed to stand at room temperature for 12 h in a standard 5 mm NMR tube. ^1H and $^{31}P\{^1H\}$ NMR indicated the clean and complete conversion of *OC*-6-34-$[IrH\{\kappa^2C,P\text{-}HN(4\text{-}C_6H_3CH_3)PPh_2\}(HNP)_2(CH_3CN)]^+$ to *OC*-6-52-$[IrH\{\kappa^2C,P\text{-}HN(4\text{-}C_6H_3CH_3)PPh_2\}(HNP)_2(CH_3CN)]^+$.

General procedure for the catalytic dehydrogenation of formic acid

The catalytic tests were carried out on a Man on the Moon kit (Series X102, https://www.manonthemoontech.com/x102-gas-evolu-tion.html), employing a reactor with a total volume of 19 mL. A DMF solution (1.7 mL) of formic acid (20 μL,

 This journal is © The Royal Society of Chemistry 2022

Open Access Article. Published on 25 July 2022. Downloaded on 1/21/2026 6:06:26 AM.
This article is licensed under a Creative Commons Attribution-NonCommercial 3.0 Unported Licence.

0.529 mmol) and sodium formate or trimethylamine (10 mol%, 0.0529 mmol; 50 mol%, 0.264 mmol) was introduced into the reactor and placed in a thermostated oil bath at 353 K. After 10 min approx., a solution of the catalyst (1 mol%, 0.00529 mmol; 5 mol%, 0.0264 mmol) in 0.3 mL of DMF was added and the recording of the curve pressure *vs.* time started (*cf.* Table 1).

DFT calculations

Molecular structure optimizations and frequencies calculations were carried out with the Gaussian09 program (revision D.01)[17] using the method B3PW91,[18] including the D3 dispersion correction scheme by Grimme with Becke–Johnson damping.[19] The def2-SVP[20] basis and pseudo potential were used for all atoms and the "ultrafine" grid was employed in all calculations. Stationary points were characterized by vibrational analysis. The structures were optimized in dichloromethane (298 K, 1 atm) using the PCM method.[21] In order to improve the accuracy of the calculated energies, in selected cases, single point energy calculations were carried out on the optimized structures of intermediates and transition states using the method M06,[22] the def2-TZVP[20] basis and pseudo potentials, where appropriate, and the SMD model[23] for the solvent (dichloromethane). Delocalization indexes (DI) were calculated using Multiwfn.[24]

Crystal structure determination

Single crystals of $SiMe_3NP$, **1**, **2**, and **6**PF_6 were obtained by slow evaporation of dichloromethane solutions of the compounds; single crystals of **12**PF_6 were grown by slow diffusion of diethyl ether into a CH_3CN solution of the compound. X-ray diffraction data were collected at 100(2) K on a SMART APEX (**1**), APEX DUO (**2**, **6**PF_6) or D8 VENTURE ($SiMe_3NP$, **12**PF_6) Bruker diffractometers with graphite-monochromated Mo-Kα radiation (λ = 0.71073 Å) using ω-scans (and φ-scans for $SiMe_3NP$ and **12**PF_6). Intensities were integrated and corrected for absorption effects with SAINT-PLUS[25] and SADABS[26] programs, both included in APEX4 package. The structures of **1**, **6**PF_6, and **12**PF_6 were solved by the Patterson method with SHELXS-97 [27] and refined by full matrix least-squares on F^2 with SHELXL-2014 [28] under WinGX.[29]

The structure of **2** was solved with the ShelXS-2013 [30] solution program using direct methods and by using Olex2 1.5-dev[31] as the graphical interface. The model was refined with olex2.refine 1.5-dev[32] using full matrix least squares minimisation on F_2. Eventually the crystal structure of **2** was refined using NoSpherA2, an implementation of NOn-SPHERical Atom-form-factors in Olex2.[33] NoSpherA2 implementation of Hirshfeld atom refinement makes use of tailor-made aspherical atomic form factors calculated on-the-fly from a Hirshfeld-partitioned electron density (ED), not from spherical-atom form factors. The ED is calculated from a gaussian basis set single determinant SCF wavefunction – either Hartree–Fock or DFT using selected funtionals – for a fragment of the crystal. This fragment can be embedded in an electrostatic crystal field by employing cluster charges or modelled using implicit solvation models, depending on the software used. The following options were used: software, Orca 5.0; partitioning, NoSpherA2; int. accuracy, normal; method, r2scan; basis set: x2c-tzvp; charge: 0; multiplicity: 1; relativistic: dkh2.

Crystal data and structure refinement for $SiMe_3N(4\text{-tolyl})PPh_2$ ($SiMe_3NP$)

$C_{22}H_{26}NPSi$, 363.50 g mol^{-1}, triclinic, $P\bar{1}$, a = 8.6970(3) Å, b = 11.2407(4) Å, c = 11.9717(4) Å, α = 117.9100(10)°, β = 97.2470(10)°, γ = 95.1980(10)°, V = 1010.90(6) Å, Z = 2, D_{calc} = 1.194 g cm^3, μ = 0.200 mm^{-1}, F(000) = 388, colourless prism, 0.190 × 0.180 × 0.120 mm, $\theta_{min}/\theta_{max}$ 2.053/28.276°, $-11 \le h \le 11$, $-14 \le k \le 13$, $-15 \le l \le 15$, reflections collected/independent 39 891/4998 [R(int) = 0.0300], T_{max}/T_{min} 0.7457/0.7210, data/restraints/parameters 4998/0/230, GooF(F^2) 1.051, R_1 = 0.0327 [$I > 2\sigma(I)$], wR_2 = 0.0876 (all data), largest diff. peak/hole 0.368/−0.261 e Å^{-3}. CCDC deposit number 2178754.†

Crystal data and structure refinement for [IrCl(HNP)(cod)] (1)

$C_{27}H_{30}ClIrNP$, 627.14 g mol^{-1}, monoclinic, $P2_1/c$, a = 18.6429(17) Å, b = 10.8746(10) Å, c = 12.3111(11) Å, β = 104.9190(10)°, V = 2411.7(4) Å^3, Z = 4, D_{calc} = 1.727 g cm^{-3}, μ = 5.728 mm^{-1}, F(000) = 1232, orange prism, 0.250 × 0.180 × 0.160 mm, $\theta_{min}/\theta_{max}$ 2.188/28.755°, $-24 \le h \le 25$, $-14 \le k \le 14$, $-16 \le l \le 16$, reflections collected/independent 33 669/5870 [R(int) = 0.0444], T_{max}/T_{min} 0.7458/0.6264, data/restraints/parameters 5870/1/285, GooF(F^2) 1.028, R_1 = 0.0270 [$I > 2\sigma(I)$], wR_2 = 0.0604 (all data), largest diff. peak/hole 1.495/−0.949 e Å^{-3}. CCDC deposit number 2178757.†

Crystal data and structure refinement for [IrCl($SiMe_3NP$)(cod)] (2)

$C_{30}H_{38}ClIrNPSi$, 699.37 g mol^{-1}, triclinic, $P\bar{1}$, a = 9.4160(10) Å, b = 10.5553(11) Å, c = 14.9182(16) Å, α = 86.0960(10)°, β = 74.7700(10)°, γ = 76.9410(10)°, V = 1393.6(3) Å^3, Z = 2, D_{calc} = 1.667 g cm^{-3}, μ = 5.007 mm^{-1}, F(000) = 696, orange prism, 0.300 × 0.190 × 0.180 mm, $\theta_{min}/\theta_{max}$ 1.41/28.37°, $-11 \le h \le 12$, $-14 \le k \le 14$, $0 \le l \le 19$, reflections collected/independent 18 124/6925 [R(int) = 0.0158], T_{min}/T_{max} 0.3302/0.2449, data/restraints/parameters 6925/21/658, GooF(F^2) 1.064, R_1 = 0.0115 [$I > 2\sigma(I)$], wR_2 = 0.0261 (all data), largest diff. peak/hole 1.092/−0.443 e Å^{-3}. CCDC deposit number 2178753.†

Crystal data and structure refinement for [IrH{κ^2*C*,*P*-$SiMe_3N(4\text{-}C_6H_3CH_3)PPh_2$}(cod)($CH_3CN$)][$PF_6$] (6$PF_6$)

$C_{32}H_{41}F_6IrN_2P_2Si$, 849.90 g mol^{-1}, triclinic, $P\bar{1}$, a = 15.413(5) Å, b = 16.528(6) Å, c = 28.517(10) Å, α = 106.793(6)°, β = 94.609(7)°, γ = 102.683(8)°, V = 6704(4) Å^3, Z = 8, D_{calc} = 1.684 g cm^{-3}, μ = 4.173 mm^{-1}, F(000) = 3376, yellow prism, 0.210 × 0.150 × 0.050 mm, $\theta_{min}/\theta_{max}$ 0.755/26.372°, $-19 \le h \le 19$, $-20 \le k \le 20$, $-35 \le l \le 35$, reflections collected/independent 121 535/27 407 [R(int) = 0.0464], T_{max}/T_{min} 0.5959/0.4686, data/restraints/parameters 27 407/4/1621, GooF(F^2) 1.018, R_1 = 0.0309 [$I > 2\sigma(I)$], wR_2 = 0.0695 (all data), largest diff. peak/hole 2.061/−0.848 e Å^{-3}. CCDC deposit number 2178755.†

Open Access Article. Published on 25 July 2022. Downloaded on 1/21/2026 6:06:26 AM.
This article is licensed under a Creative Commons Attribution-NonCommercial 3.0 Unported Licence.

Crystal data and structure refinement for [IrH{κ²*C*,*P*-HN(4-$C_6H_3CH_3$)PPh_2}$(HNP)_2(CH_3CN)$][PF_6] (12PF_6)

2[$C_{59}H_{57}IrN_4P_3$][PF_6]·3 CH_3CN·$C_4H_{10}O$, 2701.61 g mol^{-1}, monoclinic, $P2_1/c$, a = 24.8378(10) Å, b = 23.4102(8) Å, c = 20.6295(8) Å, β = 91.556(2)°, V = 11 990.8(8) Å^3, Z = 4, D_{calc} = 1.497 g cm^{-3}, μ = 2.399 mm^{-1}, $F(000)$ = 5472, colourless prism, 0.190 × 0.040 × 0.020 mm^3, $\theta_{min}/\theta_{max}$ 1.975/25.681°, index ranges $-30 \le h \le 30$, $-28 \le k \le 28$, $-25 \le l \le 25$, reflections collected/independent 337 915/22 758 [R(int) = 0.0705], T_{max}/T_{min} 0.8621/0.7473, data/restraints/parameters 22 758/10/1504, GooF(F^2) 1.056, R_1 = 0.0339 [$I > 2\sigma(I)$], wR_2 = 0.0860 (all data), largest diff. peak/hole 3.415/−0.872 e Å^{-3}. CCDC deposit number 2178756.†

Conflicts of interest

There are no conflicts to declare.

Acknowledgements

Financial support from the Spanish Ministerio de Ciencia e Innovación MCIN/AEI/10.13039/501100011033, under the project PID2019-103965GB-I00, and the Departamento de Ciencia, Universidad y Sociedad del Conocimiento del Gobierno de Aragón (group E42_20R) is gratefully acknowledged. Authors are grateful for the reviewer's insightful comments on the refinement of the crystal structure of **2** using non-spherical form factors.

References

1 (*a*) G. Ewart, D. S. Payne, A. L. Porte and A. P. Lane, *J. Chem. Soc.*, 1962, 3984; (*b*) H. H. Sisler and N. L. Smith, *J. Org. Chem.*, 1961, **26**, 611; (*c*) W. A. Hart and H. H. Sisler, *Inorg. Chem.*, 1964, **3**, 617–622.

2 (*a*) V. Passarelli, J. J. Pérez-Torrente and L. A. Oro, *Dalton Trans.*, 2016, **45**, 951–962; (*b*) J. Jansa, T. Řezníček, L. Dostál, Z. Růžičková, F. Bureš and R. Jambor, *Appl. Organomet. Chem.*, 2016, **30**, 1036–1042; (*c*) S. Pavlik, K. Mereiter, R. Schmid and K. Kirchner, *Organometallics*, 2003, **22**, 1771–1774; (*d*) A. D. Burrows, M. F. Mahon and M. T. Palmer, *J. Chem. Soc., Dalton Trans.*, 2000, 1669–1677; (*e*) L. Melounková, M. Syková, R. Jirásko, R. Jambor, R. Havelek, E. Peterová, J. Honzíček and J. Vinklárek, *New J. Chem.*, 2021, **45**, 19506–19514; (*f*) P. Chen, Y. Li, Z. Chen, W. Du and Y. Chen, *Angew. Chem., Int. Ed.*, 2020, **59**, 7083–7088; (*g*) K. G. Gaw, M. B. Smith, J. B. Wright, A. M. Z. Slawin, S. J. Coles, M. B. Hursthouse and G. J. Tizzard, *J. Organomet. Chem.*, 2012, **699**, 39–47; (*h*) M. Aydemir, A. Baysal, N. Gürbüz, I. Özdemir, B. Gümgüm, S. Özkar, N. Çaylak and L. T. Yildirim, *Appl. Organomet. Chem.*, 2010, **24**, 17–24; (*i*) S. Priya, M. S. Balakrishna and J. T. Mague, *J. Organomet. Chem.*, 2003, **679**, 116–124.

3 (*a*) Y. Chen, D. Song, J. Li, X. Hu, X. Bi, T. Jiang and Z. Hou, *ChemCatChem*, 2018, **10**, 159–164; (*b*) H. Lin, Y. Li, J. Wang, M. Zhang, T. Jiang, J. Li and Y. Chen, *Appl. Organomet. Chem.*, 2021, **35**, e6345, DOI: 10.1002/aoc.6345.

4 Selected references are: (*a*) B. S. Mitchell, W. Kaminsky and A. Velian, *Inorg. Chem.*, 2021, **60**, 6135–6139; (*b*) A. Aloisi, É. Crochet, E. Nicolas, J.-C. Berthet, C. Lescot, P. Thuéry and T. Cantat, *Organometallics*, 2021, **40**, 2064–2069; (*c*) J. A. Kephart, A. C. Boggiano, W. Kaminsky and A. Velian, *Dalton Trans.*, 2020, **49**, 16464–16473; (*d*) H. Zhang, G. P. Hatzis, C. E. Moore, D. A. Dickie, M. W. Bezpalko, B. M. Foxman and C. M. Thomas, *J. Am. Chem. Soc.*, 2019, **141**, 9516–9520; (*e*) J. A. Kephart, B. S. Mitchell, A. Chirila, K. J. Anderton, D. Rogers, W. Kaminsky and A. Velian, *J. Am. Chem. Soc.*, 2019, **141**, 19605–19610; (*f*) K. M. Gramigna, D. A. Dickie, B. M. Foxman and C. M. Thomas, *ACS Catal.*, 2019, **9**, 3153–3164; (*g*) M. L. Bin Ismail and C.-W. So, *Chem. Commun.*, 2019, **55**, 2074–2077; (*h*) B. A. Barden, G. Culcu, J. P. Krogman, M. W. Bezpalko, G. P. Hatzis, D. A. Dickie, B. M. Foxman and C. M. Thomas, *Inorg. Chem.*, 2019, **58**, 821–833; (*i*) A. J. Ayres, A. J. Wooles, M. Zegke, F. Tuna and S. T. Liddle, *Inorg. Chem.*, 2019, **58**, 13077–13089.

5 (*a*) K. A. Grice, W. Kaminsky and K. I. Goldberg, *Inorg. Chim. Acta*, 2011, **369**, 76–81; (*b*) D. Wang, M. Li, X. Chen, M. Wang, Y. Liang, Y. Zhao, K. N. Houk and Z. Shi, *Angew. Chem., Int. Ed.*, 2021, **60**, 7066–7071; (*c*) K. G. Gaw, A. M. Z. Slawin and M. B. Smith, *Organometallics*, 1999, **18**, 3255–3257.

6 Selected references are: (*a*) A. Luque-Gómez, S. García-Abellán, J. Munarriz, V. Polo, V. Passarelli and M. Iglesias, *Inorg. Chem.*, 2021, **60**, 15497–15508; (*b*) N. Onishi, R. Kanega, E. Fujita and Y. Himeda, *Adv. Synth. Catal.*, 2019, **361**, 289–296; (*c*) S.-M. Lu, Z. Wang, J. Wang, J. Li and C. Li, *Green Chem.*, 2018, **20**, 1835–1840; (*d*) S. Cohen, V. Borin, I. Schapiro, S. Musa, S. De-Botton, N. V. Belkova and D. Gelman, *ACS Catal.*, 2017, **7**, 8139–8146; (*e*) S. Siek, D. B. Burks, D. L. Gerlach, G. Liang, J. M. Tesh, C. R. Thompson, F. Qu, J. E. Shankwitz, R. M. Vasquez, N. Chambers, G. J. Szulczewski, D. B. Grotjahn, C. E. Webster and E. T. Papish, *Organometallics*, 2017, **36**, 1091–1106; (*f*) C. Fink and G. Laurenczy, *Dalton Trans.*, 2017, **46**, 1670–1676; (*g*) J. Li, J. Li, D. Zhang and C. Liu, *ACS Catal.*, 2016, **6**, 4746–4754; (*h*) J. J. A. Celaje, Z. Lu, E. A. Kedzie, N. J. Terrile, J. N. Lo and T. J. Williams, *Nat. Commun.*, 2016, **7**, 11308; (*i*) J. H. Barnard, C. Wang, N. G. Berry and J. Xiao, *Chem. Sci.*, 2013, **4**, 1234–1244; (*j*) J. F. Hull, Y. Himeda, W.-H. Wang, B. Hashiguchi, R. Periana, D. J. Szalda, J. T. Muckerman and E. Fujita, *Nat. Chem.*, 2012, **4**, 383–388; (*k*) Y. Himeda, *Green Chem.*, 2009, **11**, 2018–2022.

7 M. Iglesias and L. A. Oro, *Eur. J. Inorg. Chem.*, 2018, 2125–2138.

8 V. Passarelli and F. Benetollo, *Inorg. Chem.*, 2011, **50**, 9958–9967.

9 M. Palmese, V. Passarelli and J. J. Pérez-Torrente, *Dalton Trans.*, 2022, **51**, 7142–7153.

This journal is © The Royal Society of Chemistry 2022

Open Access Article. Published on 25 July 2022. Downloaded on 1/21/2026 6:06:26 AM.
This article is licensed under a Creative Commons Attribution-NonCommercial 3.0 Unported Licence.

10 M. Brookhart, M. L. H. Green and G. Parkin, *Proc. Natl. Acad. Sci. U. S. A.*, 2007, **104**, 6908–6914.
11 Nomenclature of Inorganic Chemistry, IUPAC Recommendations 2005, the Red Book, compiled by N. G. Connelly, R. M. Hartshorn, T. Damhus and A. T. Hutton, Published for the International Union of Pure and Applied Chemistry by The Royal Society of Chemistry, Thomas Graham House, Science Park, Milton Road, Cambridge CB4 0WF, UK ISBN 0-85404-438-8.
12 V. Passarelli, J. J. Pérez-Torrente and L. A. Oro, *Inorg. Chem.*, 2014, **53**, 972–980.
13 E. Matito, J. Poater, M. Solá, M. Duran and P. Salvador, *J. Phys. Chem. A*, 2005, **109**, 9904–9910.
14 J. L. Herde, J. C. Lambert and C. V. Senoff, *Inorg. Synth.*, 1974, **15**, 18–20.
15 V. W. Day, W. G. Klemperer and D. J. Main, *Inorg. Chem.*, 1990, **29**, 2345–2355.
16 R. Dorta, R. Goikhman and D. Milstein, *Organometallics*, 2003, **22**, 2806–2809.
17 M. J. Frisch, G. W. Trucks, H. B. Schlegel, G. E. Scuseria, M. A. Robb, J. R. Cheeseman, G. Scalmani, V. Barone, B. Mennucci, G. A. Petersson, H. Nakatsuji, M. Caricato, X. Li, H. P. Hratchian, A. F. Izmaylov, J. Bloino, G. Zheng, J. L. Sonnenberg, M. Hada, M. Ehara, K. Toyota, R. Fukuda, J. Hasegawa, M. Ishida, T. Nakajima, Y. Honda, O. Kitao, H. Nakai, T. Vreven, J. A. Montgomery Jr., J. E. Peralta, F. Ogliaro, M. Bearpark, J. J. Heyd, E. Brothers, K. N. Kudin, V. N. Staroverov, R. Kobayashi, J. Normand, K. Raghavachari, A. Rendell, J. C. Burant, S. S. Iyengar, J. Tomasi, M. Cossi, N. Rega, J. M. Millam, M. Klene, J. E. Knox, J. B. Cross, V. Bakken, C. Adamo, J. Jaramillo, R. Gomperts, R. E. Stratmann, O. Yazyev, A. J. Austin, R. Cammi, C. Pomelli, J. W. Ochterski, R. L. Martin, K. Morokuma, V. G. Zakrzewski, G. A. Voth, P. Salvador, J. J. Dannenberg, S. Dapprich, A. D. Daniels, C. Farkas, J. B. Foresman, J. V. Ortiz, J. Cioslowski and D. J. Fox, *Gaussian 09, Revision D.01*, Gaussian, Inc., Wallingford CT, 2009.
18 J. P. Perdew, in *Electronic Structure of Solids '91*, ed. P. Ziesche and H. Eschrig, Akademie Verlag, Berlin, 1991.
19 S. Grimme, S. Ehrlich and L. Goerigk, *J. Comput. Chem.*, 2011, **32**, 1456–1465.
20 F. Weigend and R. Ahlrichs, *Phys. Chem. Chem. Phys.*, 2005, **7**, 3297–3305.
21 J. Tomasi, B. Mennucci and R. Cammi, *Chem. Rev.*, 2005, **105**, 2999–3093.
22 Y. Zhao and D. G. Truhlar, *J. Chem. Phys.*, 2006, **125**, 194101.
23 A. V. Marenich, C. J. Cramer and D. G. Truhlar, *J. Phys. Chem. B*, 2009, **113**, 6378–6396.
24 T. Lu and F. Chen, *J. Comput. Chem.*, 2012, **33**, 580–592.
25 *SAINT+: Area-Detector Integration Software, version 6.01*, Bruker AXS, Madison, WI, 2001.
26 G. M. Sheldrick, *SADABS program*, University of Göttingen, Göttingen, Germany, 1999.
27 G. M. Sheldrick, *SHELXS 97, Program for the Solution of Crystal Structure*, University of Göttingen, Göttingen, Germany, 1997.
28 G. M. Sheldrick, *Acta Crystallogr., Sect. C: Struct. Chem.*, 2015, **71**, 3–8.
29 L. J. Farrugia, *J. Appl. Crystallogr.*, 2012, **45**, 849–854.
30 G. M. Sheldrick, *Acta Crystallogr., Sect. A: Found. Crystallogr.*, 2008, **64**, 339–341.
31 O. V. Dolomanov, L. J. Bourhis, R. J. Gildea, J. A. K. Howard and H. Puschmann, *J. Appl. Crystallogr.*, 2009, **42**, 339–341.
32 L. J. Bourhis, O. V. Dolomanov, R. J. Gildea, J. A. K. Howard and H. Puschmann, *Acta Crystallogr., Sect. A: Found. Adv.*, 2015, **71**, 59–71.
33 F. Kleemiss, O. V. Dolomanov, M. Bodensteiner, N. Peyerimhoff, M. Midgley, L. J. Bourhis, A. Genoni, L. A. Malaspina, D. Jayatilaka, J. L. Spencer, F. White, B. Grundkoetter-Stock, S. Steinhauer, D. Lentz, H. Puschmann and S. Grabowsky, *Chem. Sci.*, 2021, **12**, 1675–1692.
34 M. J. Church, M. J. Mays, R. N. F. Simpson and F. P. Stefanini, *J. Chem. Soc. (A)*, 1970, 2909–2914.